JOURNAL OF GEOPHYSICAL RESEARCH, VOL. 97, NO. B10, PAGES 14,115–14,135, SEPTEMBER 10, 1992

Forward and Inverse Three-Dimensional *P* Wave Velocity Models of the Southern California Crust

HAROLD MAGISTRALE,[1] HIROO KANAMORI, AND CRAIG JONES[2]

Seismological Laboratory, Division of Geological and Planetary Sciences, California Institute of Technology, Pasadena

We construct a three-dimensional *P* wave velocity model of the southern California crust by combining existing one-dimensional models, each describing a region defined by surface geology, and calibrate the model with travel times from three explosions. The model is expressed as blocks, each of a given slowness. The variance of the *P* wave travel time residuals of ≈1000 earthquakes relocated in and near the Los Angeles basin, where the model is most detailed, is half that of the catalog locations in the standard one-dimensional model for southern California. Starting from the forward model, we invert ≈21,000 *P* wave arrivals from earthquakes for hypocenters and block slownesses using the technique of Roecker (1981). The variance of these *P* wave travel time residuals decreases 47% during the inversion. Many of the blocks representing the upper crust and midcrust are well sampled and well resolved. The resulting model is useful both for locating earthquakes and for comparing the geologies of the different regions. For example, the velocity structure of the Los Angeles basin represents seismically slow sediments on top of basement rocks having velocities similar to the granitic rocks under the Peninsular Ranges. Moho is between 26 and 32 km depth. In contrast, the Ventura basin has mostly slower sediments above a deeper, higher-velocity basement. Compared to catalog locations, relocations in the final three-dimensional model of 98 $M_L \geq 4$ earthquakes throughout southern California tend to deepen below sediment filled valleys and basins, shallow in regions without sedimentary cover, and have a 44% lower *P* wave travel time residual variance.

INTRODUCTION

The southern California crust has often been assumed to be one-dimensional in studies of the seismicity of the region, yet the crust is heterogeneous. Three-dimensional velocity models can provide more accurate earthquakes locations and focal mechanisms than one-dimensional models; these improvements can better resolve seismogenic structures. Further, a better understanding of the crustal seismic velocities may help to identify the types of rocks that make up the inaccessible parts of the crust and to constrain geologic models of the evolution of the crust.

Movement along faults can juxtapose rocks with different seismic velocities, so that seismically active areas often contain lateral velocity variations. Also, deep, sediment-filled basins produce strong lateral variations in seismic velocities. These velocity variations cannot be represented in a one-dimensional velocity model. Recent studies of earthquakes in deep, sediment-filled basins in southern California have attempted to correct for the presence of thick sequences of seismically slow sediments by using hybrid one-dimensional models (e.g., *Hauksson* [1987] and *Hauksson and Jones* [1989] for the Los Angeles basin and *Magistrale et al.* [1989] for the Imperial Valley). Elsewhere in California, workers have used joint hypocenter-velocity structure methods to develop three-dimensional models of small areas covered by temporary or small aperture arrays (*Thurber* [1983] for the Coyote Lake area, *Michelini et al.* [1989] for Parkfield, *Eberhart-Phillips* [1989] for Coalinga, *Michelini et al.* [1990] and *Eberhart-Phillips et al.* [1990] for the Loma Prieta area, and *Robertson and Hauksson* [1989] for the Los Angeles basin). Others have derived three-dimensional velocity structures over small areas using tomographic inversions (*Walck and Clayton* [1987] for the Coso region, *Lees and Nicholson* [1990] for northern Coachella Valley, and *Lees* [1990] for Loma Prieta and Parkfield). These three-dimensional models were developed to study the distributions of seismic velocities near a single fault or basin or during a specific earthquake sequence. Large aperture studies of the velocity structure of the southern California crust recognized the regional variations of seismic velocity (*Hearn and Clayton* [1986*a*,*b*] used a tomographic technique and *Hadley and Kanamori* [1977], *Hadley* [1978], and *Corbett* [1984] used time-distance techniques).

Here, we develop three-dimensional velocity models of the southern California crust. First, a three-dimensional forward model of the southern California crust is constructed from existing velocity models and is calibrated with explosion travel times. Then, using this forward model as a starting model, earthquake *P* wave travel times are inverted for a three-dimensional velocity model. The velocity model encompasses the region covered by the permanent U.S. Geological Survey-California Institute of Technology (USGS-Caltech) southern California seismic array. The illustrative hypocenter determinations below are the first use of regional three-dimensional velocity models to locate southern California earthquakes.

The three-dimensional velocity models were parameterized for the codes written by Roecker and coworkers [*Roecker*, 1981, 1982; *Shedlock*, 1986; *Shedlock and Roecker*, 1987; *Roecker et al.*, 1987]. The velocity models are expressed as blocks, each having a given slowness. The blocks are defined by orthogonal vertical and horizontal interfaces.

To simplify the problem of modeling the southern California crust, we partition southern California into provinces defined by the surface geology. It is assumed that each province can be adequately described by a one-dimensional model. In the

[1] Now at Department of Geological Sciences, San Diego State University, San Diego, California.

[2] Now at Mackay School of Mines, University of Nevada, Reno.

Paper number 92JB00494.
0148-0227/92/92JB-00494$05.00

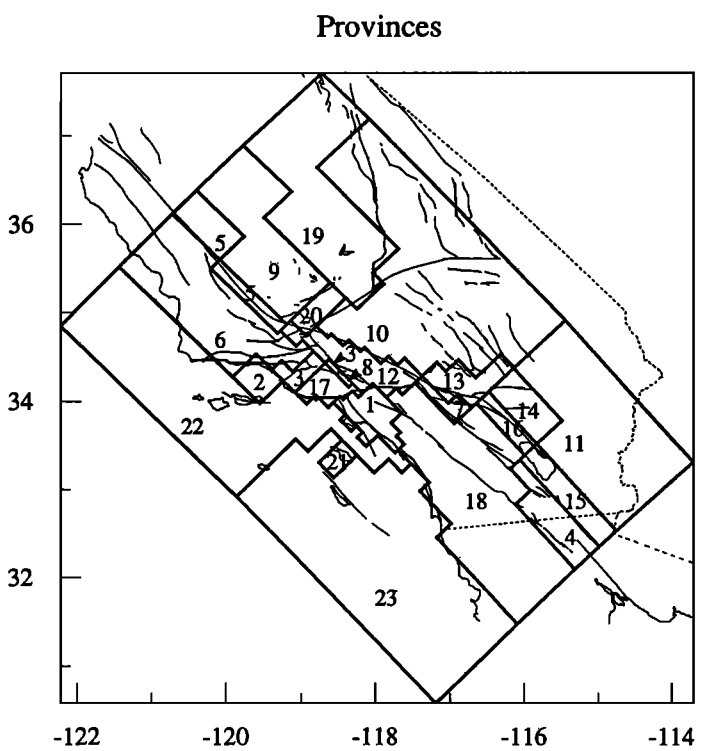

Fig. 1*a*. Three-dimensional velocity model provinces superposed on an outline of southern California. The numbers labeling the velocity provinces are keyed to the numbers in Table 1. Heavy lines are geologic province boundaries; light lines are faults. Dashed line is the California state border.

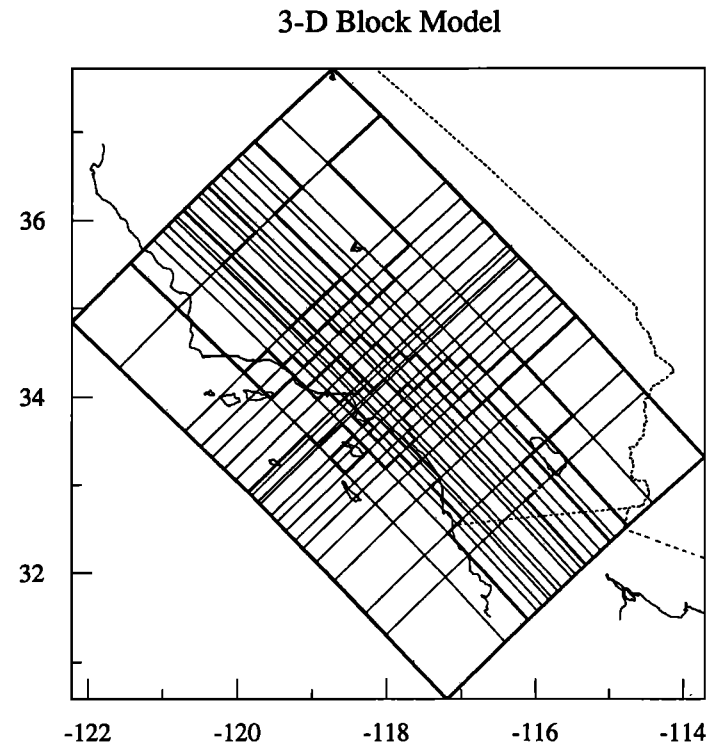

Fig. *1b*. The block model. Heavy lines outline the geologic provinces (superblocks), and light lines outline individual blocks. Twenty northwest striking and 21 northeast striking vertical interfaces and 24 horizontal interfaces are used, defining a total of 9120 blocks. Note greater detail of velocity province boundaries close to Los Angeles basin (center) and detail decreasing toward edge of model. Blocks are arranged the same way in each layer.

forward modeling, the constituent one-dimensional models are joined together to construct a three-dimensional model. In the inverse model, the provinces define the blocks that make up the three-dimensional velocity model.

FORWARD THREE-DIMENSIONAL VELOCITY MODEL

The forward model was originally developed to locate earthquakes in the Los Angeles basin. There are large contrasts between the seismic velocities of the sediments of the basin, of the crystalline rocks of the adjacent Peninsular and Transverse ranges, and of the thinner crust of the offshore region. Accurate earthquake locations are needed to study the many recent felt earthquakes within the populous Los Angeles basin and to evaluate the seismic risk of blind thrust faults beneath the basin [*Davis et al.*, 1989].

Constructing the Forward Model

The three-dimensional model was constructed by dividing southern California into 23 provinces based on surface geology and physiography (Figure 1*a*) and using a one-dimensional model for each province derived from existing seismic refraction, borehole, and earthquake and explosion travel time studies (Table 1). The one-dimensional models (Table 2) were then assembled into a three-dimensional structure.

The provinces are outlined by vertical block interfaces parallel and perpendicular to the overall structural grain of southern California. The smallest spacings between vertical interfaces, and hence the smallest blocks, outline the Los Angeles basin and the provinces nearest to the basin (Figure 1*b*), giving the three-dimensional model the most detail in and near the Los Angeles basin. Interface spacing and block size increase away from the basin because the number of seismic stations recording Los Angeles basin earthquakes decreases with distance from the basin (Figure 2). The interfaces outline 9120 blocks, but within each province (except the Los Angeles basin) the velocity structure does not vary laterally, reducing the number of independent model slownesses to 159. In the Los Angeles basin, the depth to basement varies in each column of blocks, following *Yerkes et al.* [1965].

Calibrating the Forward Model

We calibrated the three-dimensional velocity model by comparing travel times calculated in the model to the observed travel times of explosions with known origin times and locations. Calibration of the model is warranted by the greater extent of each province compared to area in which each constituent one-dimensional model was determined. Calibration also mitigates the effect of the unnaturally sharp province boundaries on the travel time residuals and corrects for any differences between near-surface velocities under the permanent seismograph stations sited on bedrock and refraction geophones often placed on alluvium. We occasionally modified the province boundaries by reassigning blocks along a boundary from one province to the adjacent province. We also tested competing one-dimensional velocity models proposed for some provinces and selected those that best fit the explosion travel times.

We calibrated the model through trial and error modifications to the velocity structures to reduce the travel time residuals for three explosions: Corona (H. Kanamori, written communication, 1989), Catalina Island [*Given and Koesterer*, 1983], and

TABLE 1. Provinces for Three-Dimensional Forward Model

Number	Province	Reference
1	Los Angeles Basin	J. Suppe (unpublished data, 1989) and H. Kanamori (written communication, 1989)
2	Santa Barbara Channel	*Crandel et al.* [1983]
3	Ventura Basin	*Corbett and Johnson* [1982]
4	Borrego Valley	*Hamilton* [1970]
5	Coast Ranges, east of San Andreas fault	*Eaton et al.* [1970]
6	Coast Ranges, west of San Andreas fault	*Walter and Mooney* [1982]
7	San Jacinto Valley	*Hadley and Combs* [1974]
8	San Fernando Valley	J. Suppe (unpublished data, 1989) and *Healy* [1963]
9	Great Valley	*Colburn and Mooney* [1986]
10	Mojave	*Kanamori and Hadley* [1975]
11	East Mojave	*Hadley* [1978]
12	San Gabriel Mountains	*Hadley and Kanamori* [1977]
13	San Bernadino Mountains	*Hadley and Kanamori* [1977]
14	Little San Bernadino Mountains	*Hadley and Kanamori* [1977]
15	Imperial Valley	*Fuis et al.* [1982]
16	Coachella Valley	*Fuis et al.* [1982] and *Hadley* [1978]
17	Santa Monica Mountains	*Stierman and Ellsworth* [1976]
18	Peninsular Ranges	H. Kanamori (written communication, 1989)
19	Sierra Nevada	*Jones and Dollar* [1986]
20	Tehachapi Mountains	P. Malin (written communication, 1989)
21	Catalina Island	*Corbett* [1984]
22	North Continental Borderland	*Corbett* [1984]
23	South Continental Borderland	*Corbett* [1984]

TABLE 2. Calibrated Velocity Models for Three-Dimensional Forward Model

Velocity, km/s	Depth, km
Los Angeles Basin	
2.65	0.0
2.90	0.4
3.40	1.0
4.00	1.5
4.50	2.1
5.50	3.0
6.40	4.0
6.80	26.0
7.80	32.0
Santa Barbara Channel	
2.00	0.0
2.19	0.5
3.23	1.5
4.90	4.0
6.36	8.0
7.01	12.0
8.33	22.0
Ventura Basin	
2.00	0.0
2.20	0.5
3.23	1.0
4.90	3.0
6.40	8.0
7.00	16.0
8.00	26.0
Borrego Valley	
2.50	0.0
5.10	0.5
6.00	3.0
7.10	14.0
7.90	25.0
Coast Ranges East of SAF	
2.85	0.0
3.34	0.5
4.62	1.5
5.62	3.0
6.00	4.0
6.80	16.0
8.05	25.0

TABLE 2. (continued)

Velocity, km/s	Depth, km
Coast Ranges West of SAF	
2.40	0.0
3.80	1.5
5.50	2.1
6.00	4.0
6.15	8.0
6.35	10.0
6.55	20.0
8.00	25.0
San Jacinto Valley	
2.29	0.0
5.30	0.5
5.80	1.5
6.20	6.0
6.80	16.0
7.80	32.0
San Fernando Valley	
2.90	0.0
3.40	1.0
4.00	1.5
4.90	2.1
6.10	3.0
7.00	14.0
8.10	26.0
Great Valley	
2.85	0.0
4.14	3.0
4.41	4.0
5.77	6.0
6.16	8.0
6.43	12.0
6.77	14.0
7.25	20.0
8.11	26.0
Mojave	
5.50	0.0
6.30	4.0
6.80	26.0
7.80	32.0

TABLE 2. (continued)

Velocity, km/s	Depth, km
East Mojave	
5.50	0.0
6.30	4.0
6.80	26.0
8.20	32.0
San Gabriel Mountains	
5.50	0.0
6.20	4.0
6.70	20.0
7.80	32.0
8.30	42.0
San Bernardino Mountains	
5.50	0.0
6.20	4.0
6.70	20.0
7.80	30.0
8.30	37.5
Little San Bernardinos	
5.50	0.0
6.20	4.0
6.70	20.0
7.80	30.0
Imperial Valley	
3.00	0.0
3.10	1.0
3.80	2.1
4.60	3.0
5.55	4.0
5.80	6.0
6.50	14.0
7.30	16.0
7.50	20.0
Coachella Valley	
3.00	0.0
3.10	1.0
3.80	2.1
5.50	3.0
6.20	8.0
7.80	20.0
Santa Monica Mountains	
3.00	0.0
6.10	0.5
6.80	14.0
8.10	30.0
Peninsular Ranges	
5.50	0.0
6.40	4.0
6.80	26.0
7.90	32.0
Sierra Nevada	
3.50	0.0
5.80	1.0
6.20	8.0
6.90	22.0
7.90	36.0
Tehachapi Mountains	
5.50	0.0
5.90	0.5
6.10	1.0
6.50	4.0
6.60	8.0
7.05	14.0
7.90	32.0
Catalina Island	
2.50	0.0
5.50	0.4
6.20	3.0
7.80	22.0
North Continental Borderland	
5.20	0.0
6.30	6.0
7.80	22.0
South Continental Borderland	
5.20	0.0
6.30	6.0
8.20	20.0
Standard 1-D Model	
5.50	0.0
6.30	5.5
6.70	16.0
7.80	37.0

Velocity is *P* wave velocity; depth is depth to top of layer.

Whittier Narrows [*Perkins*, 1988] (Figure 2). These explosions were chosen because they were in or near the Los Angeles basin, were widely recorded (Figure 2), and were accurately timed. No station corrections were used. Most of the explosion arrival times used in the calibration were picked with a precision better than ±0.1 s, though in areas of sparse station coverage some explosion arrival times with a precision of ±0.3 s were used.

In the forward and inverse modeling, an approximate ray-tracing technique is used [*Thurber and Ellsworth*, 1980]. For each source-receiver pair, a vertical plane containing the source and receiver is defined, then within each layer the slownesses of all the blocks intersecting that plane are averaged to produce a single average slowness per layer, producing the average one-dimensional structure between source and receiver. The ray path with the smallest travel time in the average one-

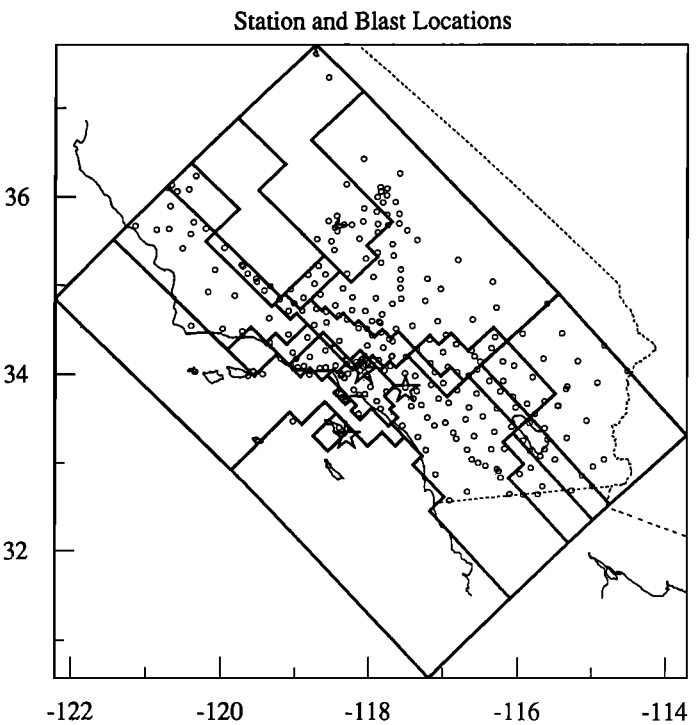

Fig. 2. Locations of explosions (stars) used to calibrate the three-dimensional model. The explosions are, from north to south, Whittier Narrows, Corona, and Catalina Island. Circles indicate seismometer locations that recorded explosion travel times for the forward model and that recorded earthquake travel times used in the inversion.

dimensional structure is found, and that ray path is followed through the full three-dimensional block model to calculate the travel time and the partial derivatives in each block hit by the ray.

Not all parts of the model are equally sampled by the explosions. Seismic rays from the blasts sample most thoroughly the upper and middle crustal layers of provinces near the Los Angeles basin. The quality of calibration decreases away from the basin. Rays reaching provinces far from the basin travel through the lower crust and Moho of several provinces, and it is hard to separate errors in velocities and Moho depths of each province from one another. These same rays spend little time in the upper layers of the distant provinces, so a meaningful calibration of the upper layers of these provinces is difficult. Also, the calibration explosions are harder to pick accurately at large distances. The offshore region is a large area of complicated geology, but has few seismometers and so has few blast observations.

In Figure 3 we compare residuals of the explosion *P* wave travel times calculated in the final forward three-dimensional velocity model to the residuals from the standard one-dimensional model (Table 2) based on work by *Kanamori and Hadley* [1975]. The one-dimensional model is used for routine earthquake locations in southern California [*Given et al.*, 1989]. The variance of the travel time residuals measures of the fit of the different models: the variances for the Whittier Narrows, Corona, and Catalina blasts are reduced by of 65%, 40%, and 32%, respectively, in the three-dimensional model (Table 3).

Application of the Forward Model

We relocated in the three-dimensional velocity model 1055 earthquakes of various magnitudes whose catalog locations are within a 45-km-wide band from Palos Verdes to the San Andreas fault (Figure 4). Most of the earthquakes are in the Los Angeles basin, with the rest in the San Gabriel Mountains and offshore. The earthquakes occurred between 1983 and 1987 and include the 1987 Whittier Narrows sequence. Routine processing [*Given et al.*, 1986] of these events recorded on the USGS-Caltech seismic network produced the *P* and *S* wave arrival times used here. During this processing, catalog hypocenters are determined by an earthquake location program [*Johnson*, 1979] in the standard one-dimensional velocity model (Table 2, based on work by *Kanamori and Hadley* [1975]) using *P* and *S* wave arrival times with no distance cutoff and some station corrections [*Given et al.*, 1989]. Our relocations are useful to judge the improvement of earthquake location quality in the three-dimensional model over the standard one-dimensional model.

During the earthquake relocations, arrivals from stations beyond 100 km are downweighted by a truncation function that smoothly scales the arrival weights from full value to zero as source-receiver distance varies from 80 km to 120 km. The 100-km cutoff distance was determined from the calibration explosion travel times, which are closely fit by the three-dimensional model at distances less than about 100 km (Figure 3). Arrivals with large residuals are also downweighted, with the residual cutoff set to 3 (1) s for the first (last) iteration. *S* wave arrivals are given one-half the weight of *P* wave arrivals, and a V_p/V_s ratio of 1.73 is assumed. No station corrections are used.

When the southern California array data are processed, the arrival time picks are assigned qualities according to the maximum error in the timing of the pick (Table 4). The location and inversion programs use arrival time weights inversely

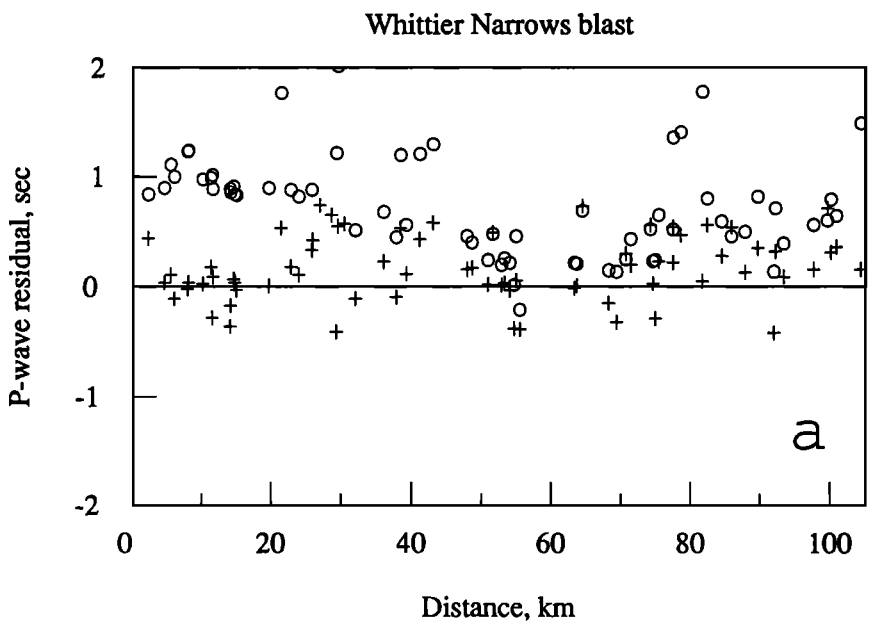

Fig. 3. *P* wave travel time residuals of the explosions calculated in the three-dimensional velocity model (crosses) and in the standard one-dimensional velocity model (circles). (a) Whittier Narrows explosion. The travel time residuals of the standard one-dimensional model are large and positive, indicating that the standard model is too fast with respect to the observed travel times. This is due in part to the lack of low velocity sediments in the standard model such as exist in the Los Angeles basin. See also Table 3. (b) Corona explosion. Note scatter of residuals for both models, but overall lower residuals for three-dimensional model. See also Table 3. (c) Catalina explosion. The residuals of the standard model are mostly negative, indicating that the standard model is too slow with respect to the observed travel times. See also Table 3.

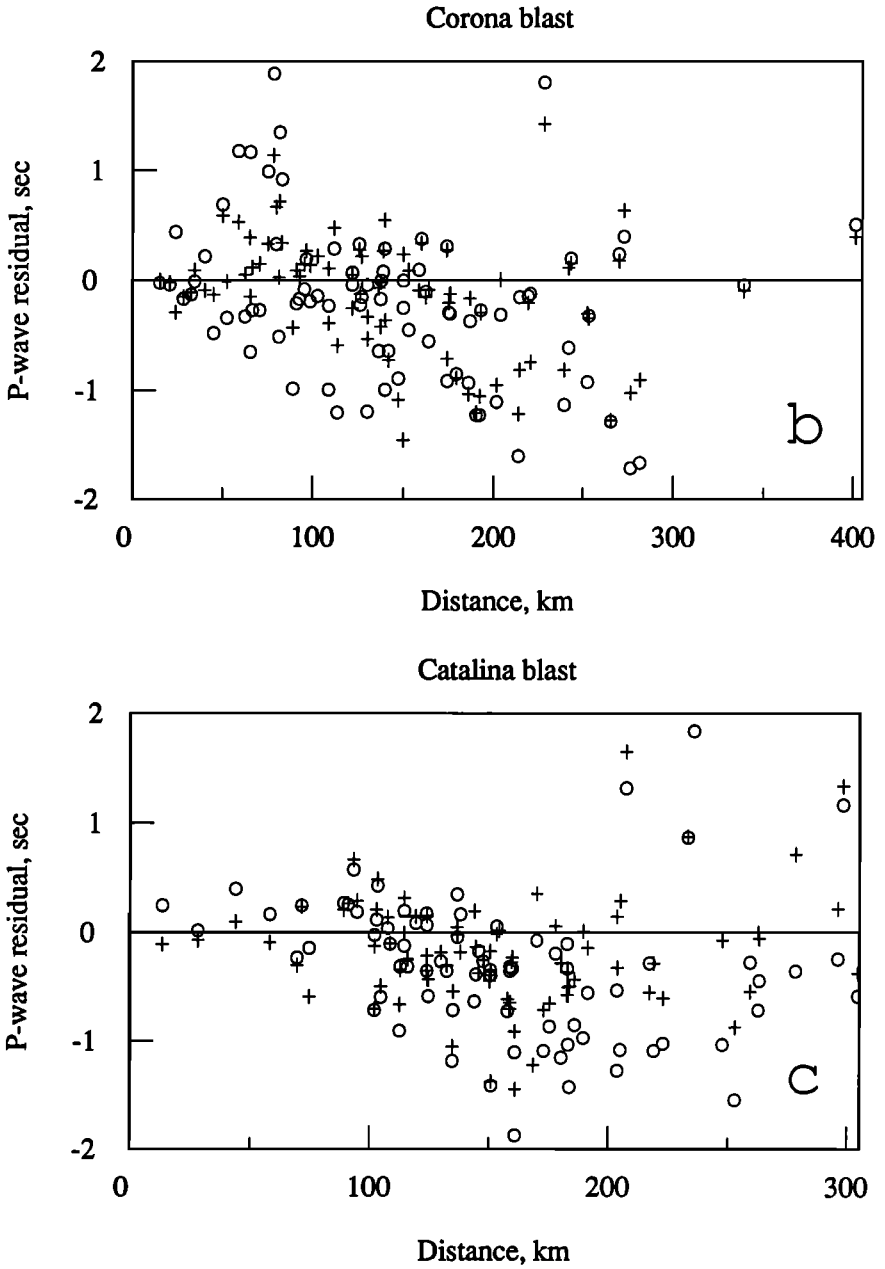

Fig. 3. (continued)

proportional to the variance of the arrival time errors. To calculate the actual weights used in the location program (Table 4), it is assumed here that the maximum errors correspond to the standard deviation of the arrival time errors. The lowest maximum error, 0.02 s, is determined by the array digitization rate. The actual weight used here for that quality pick corresponds to a maximum error of 0.03 s, a realistic value that avoids overweighting the best quality picks.

Earthquakes relocated in the three-dimensional model (Figures 4 and 5) cluster more tightly along the Newport-Inglewood and San Andreas faults, and the Whittier Narrows sequence is more compact and has a more sharply defined aftershock zone. The Newport-Inglewood fault does not appear clearly in the cross section because the cross section intersects that fault obliquely and because of the more diffuse seismicity associated with that fault compared to the San Andreas fault. The line of hypocenters at 6 km depth in the catalog location cross section is due to the fixed depth of earthquakes whose depths were problematic due, in part, to the inadequacy of the standard one-dimensional model. In the relocations depth was not fixed, and these events scatter to various depths with small (<1 km) errors. Other than the 14- to 17-km-deep Whittier Narrows sequence, the relocated earthquakes do not cluster at any particular depth.

The latitude and longitude differences between the catalog locations and the relocations are typically <1 km and average to near zero. The relocations are, on average, deeper (0.9 km for M_L 1 to 2 events and 2.4 km for $M_L \geq 3$ events) and earlier (0.22 s for M_L 1 to 2 events and 0.28 s for $M_L \geq 3$ events) than the catalog locations. The differences between the magnitude ranges are due to the larger events being recorded at more stations. The variance of the P wave travel time residuals for

TABLE 3. Blast and Earthquake Set Travel Time Residual Variances

Model	Variance, s^2	Station Corrections*	Distance Cutoff, km
	Corona		
1-D standard	0.209	no	none
3-D forward	0.127	no	none
3-D inverse start	0.042	yes	100
3-D inverse final	0.029	yes	100
	Whittier Narrows		
1-D standard	0.170	no	none
3-D forward	0.060	no	none
3-D inverse start	0.176	yes	100
3-D inverse final	0.140	yes	100
	Catalina		
1-D standard	0.353	no	none
3-D forward	0.240	no	none
3-D inverse start	0.095	yes	100
3-D inverse final	0.089	yes	100
	1055 Earthquakes in and Near Los Angeles Basin		
Catalog	0.091	no	100
3-D forward	0.048	no	100
	1041 Earthquakes and Three Blasts Used in Inversion		
3-D inverse start	0.092	yes	900
3-D inverse final	0.048	yes	900
3-D inverse start	0.101	no	900
3-D inverse final	0.055	no	900
	98 $M_L \geq 4$ Earthquakes		
Catalog	0.127	no	100
3-D inverse final	0.071	yes	100

* See Table 6.

TABLE 4. Arrival Time Weights

Arrival Quality	Maximum Error, s	Weight Used in 3-D Codes
0	0.02	1111
1	0.05	400
2	0.10	100
3	0.30	11
4	>0.30	0

the earthquakes relocated in the three-dimensional model is 47% less than the variance of the the catalog locations (Table 3). The forward three-dimensional velocity model is a clear improvement for locating earthquakes in and around the Los Angeles basin.

INVERSE THREE-DIMENSIONAL VELOCITY MODEL

The forward three-dimensional crustal velocity model is an improvement over the standard one-dimensional model and is useful for locating earthquakes in the Los Angeles basin, an area of large lateral variations of seismic velocities. That three-dimensional velocity model was calibrated by forward modeling of relatively few explosion *P* wave travel times. There is a great number of earthquake arrival times available from the southern California seismic array, and the associated ray paths sample most of the crust. Here, earthquake and explosion *P* wave travel times are inverted for a three-dimensional velocity structure of southern California. A reparameterized version of the forward model is used as the starting model in the inversion. The result is a simple velocity

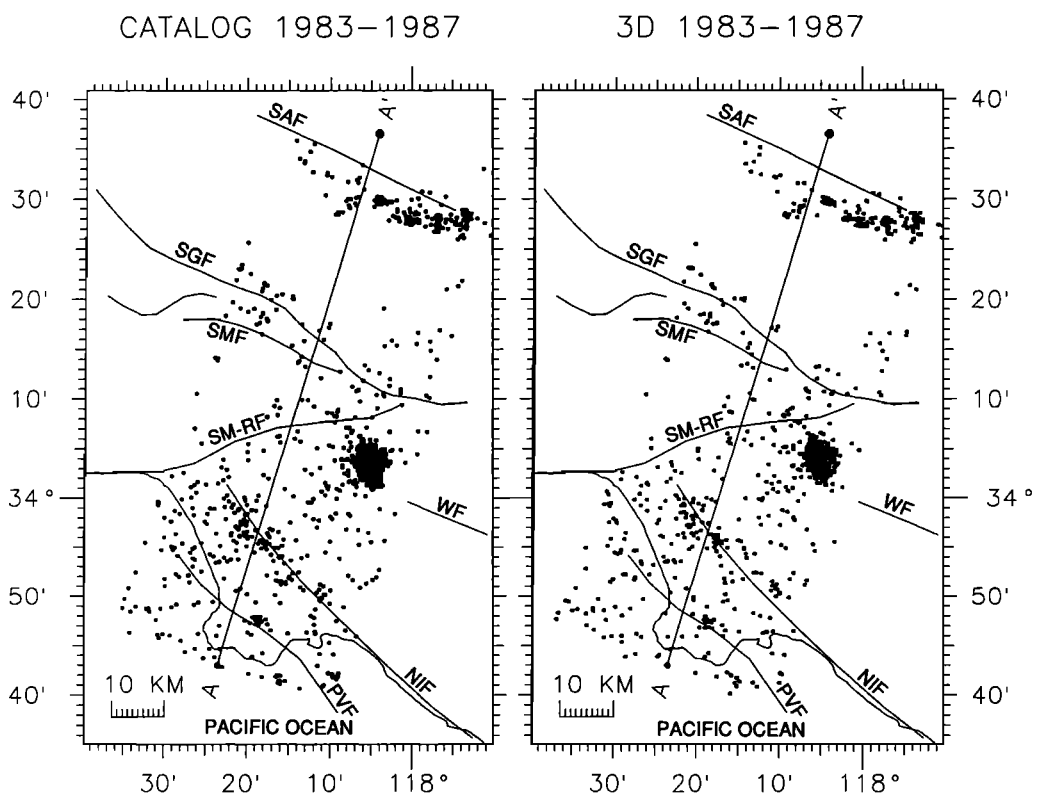

Fig. 4. (Left) Locations of 1055 earthquakes from the Caltech catalog from 1983 to 1987. (Right) The same earthquakes relocated in the forward three-dimensional velocity model. All magnitude earthquakes are plotted with the same size symbol. The 1987 Whittier earthquake sequence, mentioned in the text, is the cluster centered at 34°3', 118°6'. AA' is the location of the cross section of Figure 5. SAF, San Andreas fault; SGF, San Gabriel fault; SMF, Sierra Madre fault; SM-RF, Santa Monica-Raymond fault; WF, Whittier fault; NIF, Newport-Inglewood fault; PVF, Palos Verdes fault.

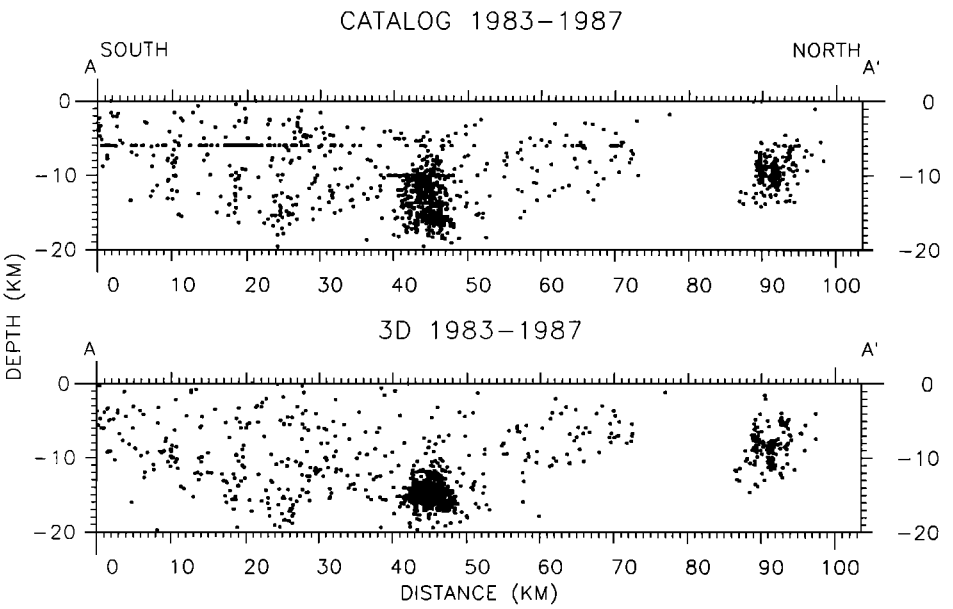

Fig. 5. The earthquakes of Figure 4 projected onto the plane AA'. (Top) The catalog locations. (Bottom) The three-dimensional relocations. All magnitude earthquakes are plotted with the same size symbol. The 1987 Whittier earthquake sequence, mentioned in the text, is the cluster centered at km 45.

model useful for geologic interpretations and for relocating earthquakes anywhere in southern California with a large residual variance reduction relative to the catalog locations.

Method

The inversion is performed using the codes HYPIT and REL3D written by Roecker and coworkers [*Roecker*, 1981, 1982; *Shedlock*, 1986; *Shedlock and Roecker*, 1987; *Roecker et al.*, 1987]. The inversion procedure minimizes travel time residuals in a damped least squares sense. As in the forward model, the three-dimensional velocity model is expressed as blocks. The inversion iteratively adjusts the seismic velocities of each block and the location of each earthquake, using the method of parameter separation to ease computational requirements. The variance of the travel time residuals is monitored at each step. The inversion procedure is stopped when the variance of the travel time residuals stops decreasing. The seismic rays are retraced at each step using the approximate ray tracing technique discussed above.

The three-dimensional forward model was developed by partitioning southern California into regions. Many vertical and horizontal interfaces were used to define the edges and layers of the geologic regions (Figure 1) in detail. This produced too many small blocks for the inversion, so the block model is reparameterized in two ways. First, the blocks within a given layer of a geologic province were connected together to form "superblocks" (as shown by the province outlines in Figure 1*a*) in a manner described by *Abers and Roecker* [1991]. Thus each geologic region is modeled as one superblock per layer. The outline of the superblocks is the same in each layer. Note that the constituent blocks of a superblock need not be contiguous. (For example, the Palos Verdes peninsula is part of the Santa Monica Mountains superblock, and the Coast Ranges east of the San Andreas fault is in two pieces.)

The second reparameterization of the velocity model reduced the number of layers from 24, as in the forward model, to eight. Fewer layers were needed because many thin layers in the forward model were either poorly sampled by seismic rays or poorly resolved and produced unreliable results in trial inversions. Sampling and resolution of the superblocks by seismic rays are much better in the eight-layer model.

The model was modified by choosing eight layers of nearly equal thickness (4 to 6 km) that best generalized the many original layers. Velocities in the top two layers of the eight-layer model were determined by matching the travel time of a vertical ray passing through the many thin upper layers of the 24-layer model. The 24-layer model allowed closely spaced variations in Moho depth, but the eight-layer starting model has the Moho at a constant 32 km depth everywhere. Some velocity interface depths of the 24-layer model had to be changed to fit the eight-layer model, removing the differences between the starting models of some geologic provinces (the San Gabriel and the San Bernardino mountains), but velocities of those provinces evolved differently during the inversion. In the 24-layer model, the Los Angeles basin had sediments of variable thickness but in the eight-layer model the basin bottom is flat at 4 km depth. The eight-layer starting model of each geologic province (each corresponding to a superblock) is shown in Table 5. The layer interfaces in the eight-layer model are at -3, 0.5, 4, 8, 14, 20, 26, and 32 km depth (Figure 6). The top layer of the model extends to a height above all the stations so rays can be traced to the stations at their true elevation. With eight layers and 23 superblocks per layer, the velocity inversion block model has 184 free parameters. The positions of the interfaces defining the blocks are fixed during the inversion. A superblock must be sampled by 200 or more seismic rays for its velocity to be inverted and changed from the starting model. This high number guarantees that an inverted block has been thoroughly sampled.

The superblock reparameterization assumes seismic velocities within a geologic region will be laterally constant and cannot resolve velocity variations over distances smaller than the size of the superblocks. To test the influence of small-scale, near-receiver variations in seismic velocity, we ran inversions both

TABLE 5. Inversion Results

Layer	Layer Depth, km	Starting Velocity, km/s	With Station Corrections		Without Station Corrections	
			Final Velocity, km/s	Resolution	Final Velocity, km/s	Resolution
			Los Angeles Basin			
1	-3 to 0.5	2.65	2.57	0.14	2.56	0.14
2	0.5 to 4	4.11	4.09	0.88	4.11	0.87
3	4 to 8	6.40	6.02	0.96	5.91	0.95
4	8 to 14	6.40	6.41	0.99	6.43	0.99
5	14 to 20	6.40	6.50	0.97	6.49	0.95
6	20 to 26	6.40	6.82	0.88	6.92	0.96
7	26 to 32	6.80	7.74	0.94	7.76	0.89
8	>32	7.80	8.02	0.97	8.08	0.97
			Santa Barbara Channel			
1	-3 to 0.5	2.00				
2	0.5 to 4	2.84				
3	4 to 8	4.90				
4	8 to 14	6.36				
5	14 to 20	7.01				
6	20 to 26	8.33				
7	26 to 32	8.33				
8	>32	8.33				
			Ventura Basin			
1	-3 to 0.5	2.00	1.55	0.19	1.85	0.18
2	0.5 to 4	3.33	4.90	0.71	5.45	0.73
3	4 to 8	4.90	5.14	0.83	5.02	0.80
4	8 to 14	6.40	5.80	0.95	5.64	0.95
5	14 to 20	7.00	6.70	0.96	6.68	0.96
6	20 to 26	7.00	7.33	0.94	7.36	0.94
7	26 to 32	8.00				
8	>32	8.00				
			Borrego Valley			
1	-3 to 0.5	2.50	2.80	0.04	3.03	0.04
2	0.5 to 4	5.10	5.14	0.58	5.56	0.59
3	4 to 8	6.00	5.99	0.90	6.04	0.90
4	8 to 14	6.00				
5	14 to 20	7.10				
6	20 to 26	7.10				
7	26 to 32	7.90				
8	>32	7.90				
			Coast Ranges, East of SAF			
1	-3 to 0.5	2.85	3.40	0.23	3.43	0.25
2	0.5 to 4	4.36	4.63	0.52	4.43	0.56
3	4 to 8	6.00	5.34	0.70	5.25	0.72
4	8 to 14	6.00	6.71	0.92	6.59	0.91
5	14 to 20	6.80				
6	20 to 26	6.80				
7	26 to 32	8.05				
8	>32	8.05				
			Coast Ranges, West of SAF			
1	-3 to 0.5	2.40	2.68	0.41	4.42	0.28
2	0.5 to 4	3.80	4.97	0.65	4.54	0.71
3	4 to 8	6.00	6.05	0.94	6.11	0.95
4	8 to 14	6.35	6.16	0.97	6.11	0.97
5	14 to 20	6.35	6.29	0.96	6.28	0.96
6	20 to 26	6.55	6.74	0.95	6.63	0.94
7	26 to 32	8.00				
8	>32	8.00				
			San Jacinto Valley			
1	-3 to 0.5	2.29	2.72	0.52	3.59	0.43
2	0.5 to 4	5.65	5.62	0.89	5.51	0.88
3	4 to 8	5.80	6.01	0.97	5.99	0.97
4	8 to 14	6.20	6.29	0.98	6.24	0.98
5	14 to 20	6.80	6.44	0.94	6.38	0.92
6	20 to 26	6.80	6.72	0.91	6.71	0.92
7	26 to 32	6.80				
8	>32	7.80			7.43	0.84

TABLE 5. (continued)

Layer	Layer Depth, km	Starting Velocity, km/s	With Station Corrections		Without Station Corrections	
			Final Velocity, km/s	Resolution	Final Velocity, km/s	Resolution
			San Fernando Valley			
1	-3 to 0.5	2.90				
2	0.5 to 4	4.28				
3	4 to 8	6.10	5.67	0.63		
4	8 to 14	6.10	6.28	0.70	6.19	0.78
5	14 to 20	7.00				
6	20 to 26	7.00				
7	26 to 32	8.10				
8	>32	8.10				
			Great Valley			
1	-3 to 0.5	2.85				
2	0.5 to 4	3.12	3.49	0.39	3.90	0.34
3	4 to 8	5.00	5.49	0.49	5.28	0.48
4	8 to 14	6.25	6.96	0.95	6.92	0.94
5	14 to 20	6.77	6.95	0.90	7.05	0.96
6	20 to 26	7.25	7.60	0.91	7.48	0.76
7	26 to 32	8.11				
8	>32	8.11				
			Mojave			
1	-3 to 0.5	5.50	5.72	0.95	5.80	0.96
2	0.5 to 4	5.50	5.67	0.93	5.28	0.89
3	4 to 8	6.30	6.07	0.99	6.08	0.99
4	8 to 14	6.30	6.24	1.00	6.24	1.00
5	14 to 20	6.30	6.43	0.99	6.31	0.96
6	20 to 26	6.30	6.31	0.68	6.41	0.68
7	26 to 32	6.80	5.85	0.58	5.76	0.59
8	>32	7.80	8.19	0.99	8.22	0.99
			East Mojave			
1	-3 to 0.5	5.50	5.60	0.74	5.07	0.28
2	0.5 to 4	5.50	5.39	0.59	5.92	0.75
3	4 to 8	6.30	6.16	0.97	6.09	0.93
4	8 to 14	6.30	6.24	0.86	6.23	0.98
5	14 to 20	6.30	6.40	0.88		
6	20 to 26	6.30				
7	26 to 32	6.80				
8	>32	8.20				
			San Gabriel Mountains			
1	-3 to 0.5	5.50	5.68	0.82	6.02	0.92
2	0.5 to 4	5.50	5.64	0.91	5.25	0.91
3	4 to 8	6.20	6.21	0.99	6.27	0.99
4	8 to 14	6.20	6.32	1.00	6.34	1.00
5	14 to 20	6.20	6.33	0.98	6.28	0.97
6	20 to 26	6.70	6.68	0.96	6.71	0.97
7	26 to 32	6.70	6.01	0.78	5.88	0.76
8	>32	7.80	7.87	0.99	7.83	0.99
			San Bernardino Mountains			
1	-3 to 0.5	5.50	5.41	0.79	5.18	0.80
2	0.5 to 4	5.50	5.66	0.90	5.61	0.89
3	4 to 8	6.20	5.99	0.99	5.95	0.99
4	8 to 14	6.20	6.09	0.99	6.09	0.99
5	14 to 20	6.20	6.24	0.96	6.21	0.93
6	20 to 26	6.70	6.47	0.92	6.49	0.88
7	26 to 32	6.70	6.81	0.67	6.86	0.69
8	>32	7.80	7.56	0.95	7.63	0.95
			Little San Bernardino Mountains			
1	-3 to 0.5	5.50	5.41	0.61	5.54	0.75
2	0.5 to 4	5.50	5.36	0.77	4.78	0.77
3	4 to 8	6.20	6.13	0.98	6.14	0.98
4	8 to 14	6.20	6.41	0.75	6.23	0.95
5	14 to 20	6.20				
6	20 to 26	6.70				
7	26 to 32	6.70				
8	>32	7.80				

TABLE 5. (continued)

Layer	Layer Depth, km	Starting Velocity, km/s	With Station Corrections		Without Station Corrections	
			Final Velocity, km/s	Resolution	Final Velocity, km/s	Resolution
			Imperial Valley			
1	-3 to 0.5	3.00				
2	0.5 to 4	3.59				
3	4 to 8	5.67				
4	8 to 14	5.80				
5	14 to 20	7.00				
6	20 to 26	7.50				
7	26 to 32	7.50				
8	>32	7.50				
			Coachella Valley			
1	-3 to 0.5	3.00				
2	0.5 to 4	3.72				
3	4 to 8	5.50	6.02	0.93	6.43	0.95
4	8 to 14	6.20	6.22	0.95	6.26	0.93
5	14 to 20	6.20	5.97	0.75	6.23	0.73
6	20 to 26	7.80				
7	26 to 32	7.80				
8	>32	7.80				
			Santa Monica Mountains			
1	-3 to 0.5	3.00	4.47	0.26	5.66	0.21
2	0.5 to 4	6.10	6.15	0.94	5.96	0.92
3	4 to 8	6.10	6.08	0.95	5.93	0.93
4	8 to 14	6.10	6.30	0.98	6.35	0.98
5	14 to 20	6.80	6.60	0.97	6.53	0.97
6	20 to 26	6.80	6.86	0.95	6.88	0.97
7	26 to 32	6.80				
8	>32	8.10	8.09	0.94	8.05	0.94
			Peninsular Ranges			
1	-3 to 0.5	5.50	5.62	0.77	5.69	0.87
2	0.5 to 4	5.50	5.84	0.95	5.85	0.95
3	4 to 8	6.40	6.25	0.99	6.19	0.99
4	8 to 14	6.40	6.36	1.00	6.36	1.00
5	14 to 20	6.40	6.57	0.99	6.62	0.99
6	20 to 26	6.40	6.88	0.99	6.90	0.99
7	26 to 32	6.80	7.28	0.98	7.17	0.97
8	>32	7.90	7.37	0.98	7.30	0.98
			Sierra Nevada			
1	-3 to 0.5	3.50	3.86	0.45	5.46	0.50
2	0.5 to 4	5.80	5.87	0.83	5.60	0.76
3	4 to 8	5.80	6.14	0.95	6.08	0.95
4	8 to 14	6.20	6.42	0.98	6.33	0.98
5	14 to 20	6.20	6.21	0.81	6.37	0.95
6	20 to 26	6.90	6.95	0.85		
7	26 to 32	6.90				
8	>32	7.90				
			Tehachapi Mountains			
1	-3 to 0.5	5.50	5.69	0.25	5.68	0.52
2	0.5 to 4	6.10	5.91	0.73	5.65	0.68
3	4 to 8	6.50	6.29	0.90	6.38	0.93
4	8 to 14	6.60	6.39	0.97	6.35	0.97
5	14 to 20	7.05	6.73	0.96	6.65	0.96
6	20 to 26	7.05				
7	26 to 32	7.05				
8	>32	7.90				
			Catalina Island			
1	-3 to 0.5	2.50	2.91	0.12	3.08	0.11
2	0.5 to 4	5.50	5.67	0.77	5.74	0.75
3	4 to 8	6.20	6.10	0.68	6.21	0.74
4	8 to 14	6.20				
5	14 to 20	6.20				
6	20 to 26	7.80				
7	26 to 32	7.80				
8	>32	7.80				

TABLE 5. (continued)

Layer	Layer Depth, km	Starting Velocity, km/s	With Station Corrections: Final Velocity, km/s	With Station Corrections: Resolution	Without Station Corrections: Final Velocity, km/s	Without Station Corrections: Resolution
			North Continental Borderland			
1	-3 to 0.5	5.20	4.43	0.06	4.57	0.05
2	0.5 to 4	5.20	5.81	0.94	5.74	0.87
3	4 to 8	5.20	5.75	0.91	5.95	0.94
4	8 to 14	6.30	6.31	0.98	6.26	0.98
5	14 to 20	6.30	6.72	0.96	6.77	0.97
6	20 to 26	7.80	7.12	0.93	7.12	0.97
7	26 to 32	7.80	7.98	0.96	7.54	0.77
8	>32	7.80	8.08	0.93	8.16	0.95
			South Continental Borderland			
1	-3 to 0.5	5.20	5.09	0.02	4.73	0.02
2	0.5 to 4	5.20	5.49	0.68	5.18	0.59
3	4 to 8	5.20	5.92	0.81	6.25	0.88
4	8 to 14	6.30	6.46	0.93	6.27	0.89
5	14 to 20	6.30	6.36	0.60	6.60	0.63
6	20 to 26	8.20	7.98	0.81	8.08	0.93
7	26 to 32	8.20				
8	>32	8.20				

A blank entry indicates that the block did not have its velocity inverted.

with and without station corrections. The station corrections (Table 6) were calculated from the weighted average residuals of the earthquake travel times in the starting eight-layer model. The mean correction for stations within each superblock are near zero, so the corrections are not compensating for an incorrect velocity of the superblock on which the stations stand but represent conditions truly local to the station. The station corrections decreased the variance of the travel time residuals by about 10% in the starting model (Figure 7 and Table 3), but the percentage variance decrease during each iteration of the inversion was similar for the runs with and without the corrections (Figure 7). This, and the similarity of the results found with and without the corrections, confirms that the station corrections account for local variations below the scale of the superblocks and that the inverted velocities are independent of the local conditions. Because of lower variance we prefer the results with the station corrections over those without the station corrections.

Different distance cutoffs were used on the arrival times for the earthquake relocations and the velocity inversion steps. For the earthquake locations, the distance cutoff was 100 km to get the best quality locations. With that cutoff, the seismic rays used for the locations sample only the better constrained parts of the velocity model (the middle and upper crust). For the inversion the distance cutoff was set to 900 km, purposely larger than the model. This was done to include all P_n arrivals in the inversion to improve resolution in the relatively poorly sampled lower crust and uppermost mantle. Arrivals with large residuals are also downweighted with the residual cutoff set to 3 s for the velocity inversion and set to 3 (1) s for the first (last) iteration during the earthquake relocations.

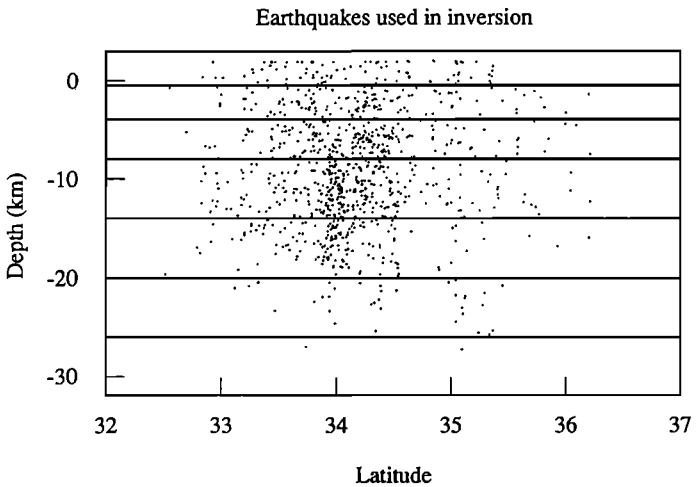

Fig. 6. Depth distribution of the earthquakes (dots) used in the inversion. The depths are calculated in the starting eight-layer model. The horizontal lines are the interfaces of the eight-layer velocity model.

Data

We desired well-located earthquakes in order to have accurate travel times to put into the inversion. Travel time residuals of poorly located earthquakes may reflect location errors rather than the velocity variations of interest. We sorted the USGS-Caltech earthquake catalog to find earthquakes well distributed in latitude, longitude, and depth occurring between 1978 and 1988. Earthquakes with fewer than 10 S and P wave arrivals were discarded, and the best quality arrival times from multicomponent stations were selected. The latter step avoids overweighting of multicomponent stations that may have several arrival time picks. We relocated the remaining earthquakes in the forward three-dimensional model (with 24 layers) using the arrivals determined from routine processing. We discarded earthquakes with horizontal or vertical location errors of $\geq$ 10 km, an azimuthal gap to receivers of $\geq$180°, or a large condition number (the ratio of the largest to the smallest eigenvalue). The first two criteria directly indicate poor quality locations, and the third warns of lack of control over one of the hypocenter parameters. The remaining 1041 earthquakes (Figure 8), with about 21,300 P wave travel times (Figure 9), were relocated in the eight-layer model with the superblock reparameterization to generate the travel times used in the first iteration of the inversion. The 245 travel times from the three explosions discussed above were also used, but these explosion locations were held fixed.

TABLE 6. Station Information

Station	Latitude		Longitude		Correction, s
ABL	34	51.05	-119	13.25	-0.06
ACO	34	4.79	-118	11.26	0.00
ADL	34	33.38	-117	25.02	0.24
AGC	32	56.47	-116	16.53	0.00
ALB	33	44.17	-117	24.16	0.00
ARC	34	6.92	-118	2.53	0.00
ARV	35	7.63	-118	49.76	0.19
BAR	32	40.80	-116	40.30	-0.06
BAT	33	27.54	-115	50.46	-0.07
BC2	33	39.42	-115	27.67	0.05
BCH	35	11.10	-120	5.05	-0.14
BCM	33	39.32	-115	26.88	0.00
BHM	34	16.73	-116	36.91	0.00
BHR	34	0.51	-118	21.72	0.00
BLK	35	5.28	-117	13.11	-0.04
BLU	34	24.40	-117	43.61	-0.04
BMT	35	8.15	-118	35.81	-0.02
BNP	37	57.31	-118	18.10	0.00
BON	32	41.67	-115	16.11	0.09
BOO	34	52.08	-117	54.62	0.21
BOW	32	50.52	-116	13.52	0.00
BRG	33	10.27	-116	10.44	0.24
BRT	34	36.69	-117	57.78	-0.03
BTL	34	15.43	-117	0.29	0.06
CAG	32	58.67	-116	25.61	0.00
CAH	33	30.22	-116	41.91	-0.12
CAL	35	6.21	-117	56.86	0.10
CAM	34	15.27	-119	2.00	-0.32
CAV	35	3.14	-116	20.35	0.00
CBK	32	54.94	-116	15.16	0.16
CFL	34	19.97	-118	1.38	-0.09
CFT	34	2.11	-117	6.66	-0.12
CH2	33	17.77	-115	20.17	-0.34
CHA	33	0.80	-116	31.57	0.00
CIS	33	24.40	-118	24.20	-0.03
CIW	33	27.92	-118	33.10	-0.06
CJP	34	10.92	-118	59.19	0.00
CJV	34	31.83	-118	8.67	-0.05
CKC	34	8.18	-117	10.48	0.10
CLC	35	49.00	-117	35.80	0.09
CLP	34	5.33	-118	57.85	0.00
CO2	33	50.83	-115	20.68	-0.11
COA	32	51.81	-115	7.36	-0.28
COQ	33	51.63	-117	30.58	0.02
COX	33	52.35	-115	19.68	0.00
COY	33	21.63	-116	18.56	0.11
CPC	34	51.46	-119	12.50	0.00
CPD	34	57.23	-119	25.10	0.00
CPE	32	52.80	-117	6.00	-0.07
CPM	34	9.24	-116	11.80	0.27
CPT	33	18.20	-117	20.40	-0.15
CRG	35	14.53	-119	43.40	0.19
CRR	32	53.18	-115	58.10	-0.05
CSP	34	17.87	-117	21.33	-0.04
CTW	33	40.78	-115	52.31	0.03
CWC	36	26.35	-118	4.68	0.46
CZA	35	3.25	-119	31.17	0.00
CZB	35	8.49	-119	38.78	0.00
CZC	35	13.48	-119	42.58	0.00
DAC	36	16.62	-117	35.62	0.00
DB2	33	44.10	-117	3.72	-0.09
DBM	34	58.74	-118	21.63	0.07
DRS	33	27.84	-116	58.21	0.00
DTP	35	16.05	-117	50.72	-0.14
DYC	33	17.11	-116	49.35	0.00
ECF	34	27.48	-119	5.44	-0.05
ECP	34	10.61	-118	5.78	0.00
EES	34	59.00	-117	34.73	0.00
ELM	34	31.57	-117	38.41	0.07
ELR	33	8.84	-115	49.95	0.32
ELS	33	38.87	-117	25.63	-0.04
EMS	32	44.48	-114	59.27	0.00
ERP	32	44.61	-115	39.76	0.00

TABLE 6. (continued)

Station	Latitude		Longitude		Correction, s
EWC	33	56.24	-116	22.86	-0.27
FAL	34	18.59	-117	48.55	-0.15
FIL	34	25.43	-118	50.07	-0.07
FLA	33	52.28	-117	58.53	0.23
FLS	34	58.22	-117	2.31	-0.02
FMA	33	42.75	-118	17.47	0.16
FMP	35	11.51	-117	34.59	0.00
FOX	34	43.98	-118	13.84	0.10
FRG	33	45.43	-116	3.69	0.06
FRI	36	59.50	-119	42.50	0.40
FRK	33	24.05	-115	38.21	-0.04
FTC	34	52.25	-118	53.51	-0.05
GAV	34	1.35	-117	30.74	-0.01
GFP	34	7.76	-118	18.59	-0.08
GLA	33	3.10	-114	49.60	-0.07
GOH	34	43.71	-118	54.64	0.00
GRI	34	7.10	-118	17.90	0.00
GRP	34	48.26	-115	36.27	0.04
GSA	34	8.22	-118	7.62	0.04
GSC	35	18.10	-116	48.30	0.17
GVF	34	3.00	-118	7.13	0.25
GWV	36	11.20	-116	40.23	0.08
HAY	33	42.40	-115	38.20	-0.05
HCM	33	59.64	-118	22.98	0.00
HDG	34	25.73	-116	18.30	0.02
HOD	34	50.33	-117	14.75	0.01
HOT	33	18.85	-116	34.90	0.00
HUN	34	7.74	-118	7.00	0.00
HYS	34	51.83	-117	34.12	0.00
IKP	32	38.93	-116	6.48	0.07
IND	33	48.97	-116	13.78	-0.32
INS	33	56.14	-116	11.66	-0.15
IPC	33	58.24	-118	20.07	0.00
IRC	34	23.31	-118	24.09	0.02
IRN	34	9.60	-115	11.04	-0.07
ISA	35	39.80	-118	28.40	-0.14
JAS	37	56.80	-120	26.30	0.98
JAW	35	18.95	-118	2.69	-0.06
JFS	35	21.05	-117	40.20	0.06
JNH	34	26.85	-117	57.27	-0.07
JRH	34	48.50	-117	41.50	0.00
JUL	33	2.90	-116	36.77	-0.13
KEE	33	38.30	-116	39.19	0.08
KIN	34	10.90	-118	4.84	0.00
KYP	34	6.11	-118	52.77	-0.10
LAN	34	43.62	-118	3.06	0.19
LAQ	33	37.68	-116	16.78	0.19
LAV	34	45.95	-116	17.19	-0.04
LCL	33	49.98	-118	12.42	-0.06
LCM	34	1.07	-118	17.22	0.00
LED	34	28.06	-115	56.19	0.02
LEO	34	37.88	-118	18.22	-0.11
LHU	34	40.30	-118	24.70	-0.03
LJB	34	35.47	-117	50.88	-0.01
LLN	34	29.07	-117	50.43	-0.03
LNA	33	47.35	-118	3.27	0.00
LOK	34	43.47	-119	5.48	0.10
LOW	34	48.71	-119	1.00	0.00
LRM	35	28.64	-117	41.35	-0.01
LRR	34	31.56	-118	1.66	0.10
LSM	36	44.32	-116	16.68	0.00
LTC	33	29.34	-115	4.20	-0.33
LTM	33	54.90	-114	55.10	0.80
LUC	34	27.30	-116	57.78	0.00
LVB	34	36.32	-117	51.88	0.00
MAR	35	0.15	-119	20.36	-0.07
MDA	33	54.78	-116	59.97	-0.16
MEC	33	38.12	-116	1.71	0.16
MIR	33	24.97	-116	4.86	0.19
MLL	34	5.48	-116	56.18	-0.01
MNP	37	24.90	-119	43.70	0.00
MON	34	8.19	-118	1.50	0.00
MOV	34	9.35	-116	30.10	0.10

TABLE 6. (continued)

Station	Latitude		Longitude		Correction, s
MRV	34	3.68	-116	32.58	-0.31
MTU	37	21.20	-118	33.81	0.00
MWC	34	13.40	-118	3.50	0.04
NAR	34	1.92	-118	3.29	0.00
NW2	33	5.43	-115	41.54	0.05
OBB	33	10.04	-115	38.20	-0.24
OLY	33	25.88	-117	7.05	-0.09
ORK	33	33.97	-115	46.15	0.00
PAD	35	38.36	-120	51.86	-0.05
PAR	36	14.95	-120	20.52	0.13
PAS	34	8.95	-118	10.29	0.06
PCF	34	3.19	-117	47.44	0.07
PCR	36	5.63	-120	26.08	-0.02
PEC	33	53.51	-117	9.60	0.03
PEM	34	10.04	-117	52.18	0.12
PHC	35	40.93	-121	9.15	0.00
PIR	33	31.42	-117	12.78	0.00
PIU	34	44.42	-115	5.64	0.00
PIV	35	54.39	-120	40.94	0.12
PKM	34	53.75	-119	49.13	-0.25
PLE	34	58.11	-119	4.08	0.29
PLM	33	21.20	-116	51.70	0.04
PMC	35	43.48	-120	22.23	0.07
PMG	35	25.79	-120	31.22	0.00
PNM	33	58.64	-115	48.05	0.08
POB	33	41.20	-116	55.40	-0.03
POC	34	6.00	-117	42.86	0.00
PPR	35	38.86	-120	42.04	0.02
PPT	36	6.50	-120	43.27	-0.15
PRI	36	8.50	-120	39.90	-0.14
PSH	35	35.45	-120	24.92	-0.06
PSM	36	4.18	-120	35.68	-0.01
PSP	33	47.63	-116	32.93	-0.01
PTD	34	0.25	-118	48.38	0.05
PTR	35	39.28	-120	12.67	0.14
PVR	33	45.13	-118	22.23	0.04
PYR	34	34.08	-118	44.50	0.11
QAL	34	44.98	-118	42.88	-0.01
RAY	34	2.18	-116	48.67	0.03
RCH	34	18.44	-116	21.03	0.01
RCP	33	46.66	-118	8.00	0.01
RDM	34	24.00	-117	11.10	0.00
RHC	34	0.47	-118	1.47	0.00
RMR	34	12.77	-116	34.52	0.04
ROD	34	37.78	-116	36.29	0.12
ROS	34	5.74	-118	3.77	0.00
RRC	33	39.92	-117	17.48	0.00
RUN	32	58.33	-114	58.63	0.03
RVM	34	10.81	-114	12.02	-0.12
RVR	33	59.60	-117	22.50	0.00
RVS	34	3.08	-114	31.08	0.20
RYS	34	38.60	-119	21.10	-0.33
SAD	34	4.86	-118	39.90	-0.01
SAT	33	42.47	-117	53.43	0.05
SAY	33	9.50	-116	40.53	0.00
SBAI	34	0.80	-119	26.23	0.24
SBB	34	41.30	-117	49.50	0.04
SBC	34	26.50	-119	42.80	-0.04
SBCC	34	56.38	-120	10.32	-0.07
SBCD	34	22.12	-119	20.63	0.01
SBI	33	28.84	-119	1.72	0.20
SBK	35	4.73	-117	34.88	0.01
SBLC	34	29.79	-119	42.81	0.77
SBLG	34	6.87	-119	3.85	0.10
SBLP	34	33.57	-120	24.02	0.29
SBSC	33	59.68	-119	37.99	0.00
SBSM	34	2.24	-120	21.01	0.04
SBSN	33	14.68	-119	30.38	-0.04
SCC	34	56.38	-120	10.32	0.12
SCD	34	22.12	-119	20.63	-0.07
SCI	32	58.80	-118	32.80	0.29
SCY	34	6.37	-118	27.25	0.03
SDL	35	22.83	-117	53.20	0.00
SDW	34	36.55	-117	4.45	-0.07
SFD	34	7.10	-117	56.59	0.00
SGL	32	38.95	-115	43.52	-0.05

TABLE 6. (continued)

Station	Latitude		Longitude		Correction, s
SHH	34	11.26	-115	39.27	-0.03
SIL	34	20.87	-116	49.60	0.05
SIP	34	12.24	-118	47.94	0.10
SJQ	33	37.20	-117	50.70	0.00
SLC	34	29.79	-119	42.81	-0.15
SLG	34	6.87	-119	3.85	-0.21
SLP	34	33.57	-120	24.02	0.00
SLT	33	15.89	-115	55.39	0.00
SMD	34	10.44	-118	3.21	0.00
SME	33	49.36	-117	21.32	-0.02
SMO	33	32.15	-116	27.70	-0.02
SNC	35	8.58	-118	18.13	-0.15
SNS	33	25.90	-117	32.90	0.27
SPA	34	6.31	-118	10.48	0.00
SPC	33	33.78	-118	8.37	0.80
SPM	34	28.32	-115	24.16	0.18
SRT	35	41.51	-117	44.96	0.33
SS2	34	12.46	-117	29.98	0.03
SSC	33	59.68	-119	37.99	0.03
SSK	34	12.97	-117	41.32	0.11
SSM	34	2.24	-120	21.01	0.02
SSN	33	14.68	-119	30.38	0.06
STT	34	47.31	-118	27.71	0.26
SUN	34	12.64	-117	41.58	0.05
SUP	32	57.31	-115	49.43	-0.18
SWM	34	43.00	-118	35.00	0.02
SYP	34	31.63	-119	58.67	0.09
SYS	32	34.78	-116	54.69	0.00
TAM	34	22.92	-117	41.07	0.00
TCC	33	59.67	-118	0.77	0.12
TEJ	35	13.79	-118	41.37	0.17
THC	34	54.52	-118	39.81	-0.05
TJR	35	1.65	-118	44.55	-0.04
TMB	35	5.24	-119	32.08	0.20
TOW	35	48.50	-117	45.90	0.46
TPC	34	6.35	-116	2.92	-0.05
TPO	34	52.73	-118	13.66	0.10
TPRM	34	5.33	-118	35.20	0.00
TTM	34	20.12	-114	49.65	-1.07
TWL	34	16.70	-118	35.67	0.21
VG2	33	49.91	-116	48.55	0.00
VPD	33	48.90	-117	45.70	-0.05
VST	33	9.40	-117	13.90	0.02
WAS	35	44.29	-118	33.42	-0.15
WBM	35	36.48	-117	53.40	0.11
WBS	35	32.22	-118	8.37	-0.13
WCH	35	52.98	-118	4.48	-0.23
WCO	35	37.35	-118	26.25	0.00
WCP	36	4.26	-117	51.01	0.06
WCS	36	1.58	-117	46.01	0.26
WCX	35	42.63	-117	35.98	-0.02
WHF	35	41.77	-118	20.91	0.04
WHP	34	18.42	-114	29.75	0.00
WHS	36	6.30	-117	45.67	0.49
WHV	35	30.60	-118	31.07	-0.02
WIS	33	16.56	-115	35.58	-0.01
WJP	35	24.65	-118	28.84	-0.07
WKT	35	47.64	-118	26.55	0.06
WLH	36	9.14	-118	18.70	0.15
WLK	33	3.08	-115	29.44	0.11
WMF	36	7.05	-117	51.17	0.32
WNM	35	50.57	-117	54.29	-0.10
WOF	35	32.14	-118	42.75	-0.24
WOR	35	41.79	-118	14.52	0.02
WRC	35	57.04	-117	38.89	0.25
WRV	36	0.47	-117	53.42	0.12
WSC	35	42.26	-117	53.19	-0.09
WSH	35	37.96	-117	29.50	-0.17
WSP	34	35.77	-118	34.72	-0.01
WVP	35	56.98	-117	49.02	0.18
WWP	35	44.13	-118	5.22	-0.06
WWR	33	59.51	-116	39.36	0.00
XMS	35	31.40	-117	21.28	0.06
YAQ	33	10.08	-116	21.00	0.19
YEG	35	26.18	-119	57.56	0.26
YUH	32	38.86	-115	55.38	0.10

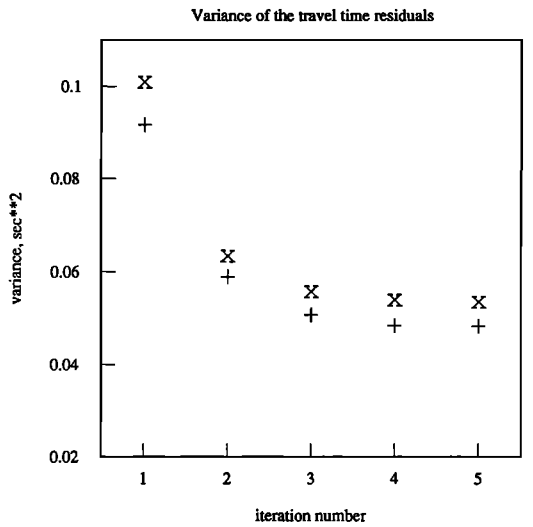

Fig. 7. Variance of the *P* wave travel time residuals versus iteration during the inversion. Variance is shown for inversions with (pluses) and without (crosses) station corrections (see text).

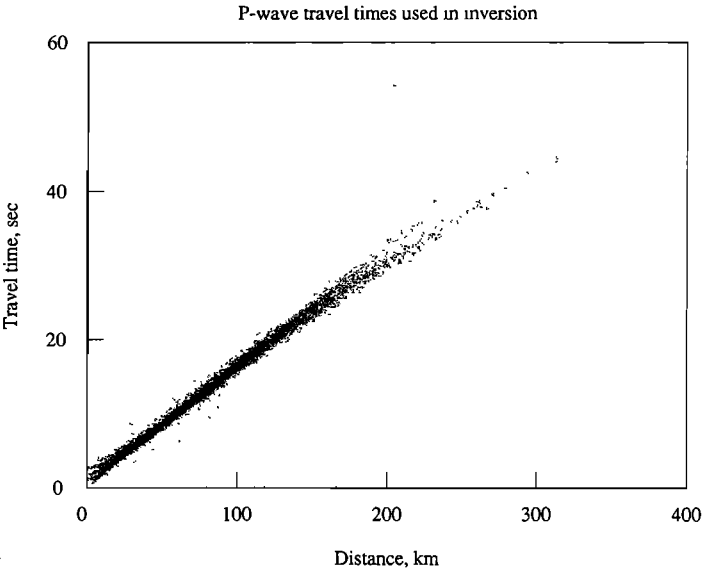

Fig. 9. The travel times used in the inversion. About 21,300 points are shown. Note that both P_n and P_g are present beyond about 150 km. Outlying points are ignored by the inversion.

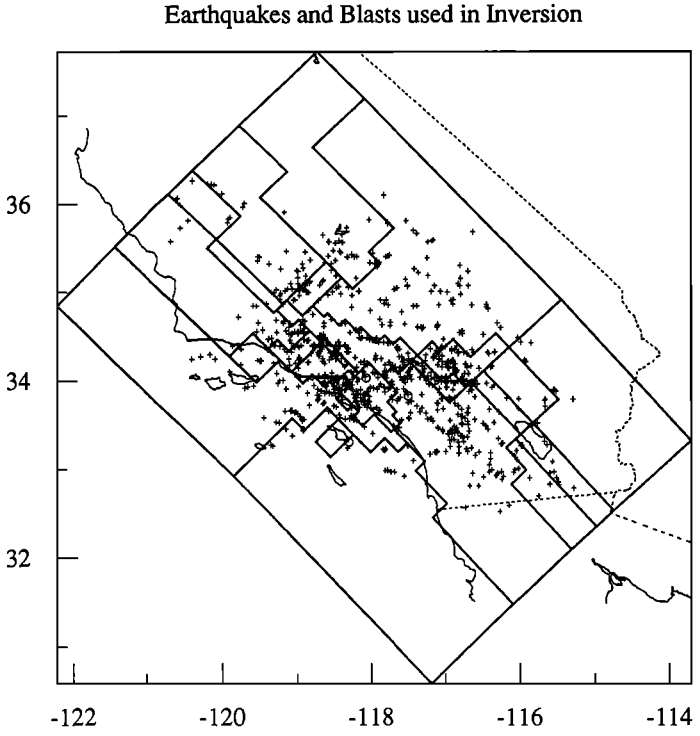

Fig. 8. The 1041 earthquakes (crosses) and three explosions (circles) that generated travel times used in the inversion. The earthquake locations are from the catalog.

The poorly located earthquakes that were discarded were mostly around the edge of the southern California seismic array, where earthquakes have poor azimuthal coverage and few close stations. In general, earthquakes near the center of the array are the best located. The three-dimensional model is centered over the array, so the lack of earthquakes and stations near the edges of the model means that few seismic rays go through the blocks near the edge of the model, especially blocks representing the lower crust and Moho. Those blocks may be poorly constrained in the inversion. Blocks containing earthquakes tend to be well constrained by the inversion. Most earthquakes in southern California are above 20 km (Figure 6), so blocks representing the crust deeper than 20 km and some blocks representing the very top of the crust, above most earthquakes, may thus not be well constrained.

In the *P* wave travel times used in the inversion (Figure 9), note that both P_g and P_n can been seen beyond about 150 km. Only first arrivals are picked during processing. This means that for some arrivals, the first arrival P_n was overlooked and the later arriving, larger-amplitude P_g was picked instead. This may cause the inverted P_n velocities to be lower than reality. Closer than 150 km the data are generally well-behaved. The data far off the *P* branch are ignored by the inversion via the large residual cutoff.

Results

Five iterations of earthquake relocations and superblock velocity adjustments were run. The last iteration's results (Table 5 and Figure 10) did not vary significantly from the penultimate iteration. The inversion reduced the variances of the travel time residuals in the models with and without the station corrections by 47% and 46%, respectively, compared to the starting models (Table 3). With the station corrections, 119 of the 184 superblocks of the model were inverted, and 117 superblocks were inverted in the runs without the station corrections (not all the superblocks had the minimum required number of hits). The blocks that changed velocity during the inversion to reduce the travel time residual variance are distributed throughout the model rather than concentrated in any area. The block boundaries are fixed during the inversion, so a resulting velocity is an average for the block. For example, a block straddling the Moho that is evenly sampled by uniform quality data will have a velocity that is an average of the true lower crust and upper mantle velocities contained in that block.

The reliability and believability of the inversion results can be judged in several ways. The model resolution matrix (Table 5) indicates both how uniquely an inverted velocity represents the true velocity within a block and how much the inverted velocity depends on the data versus depending on the starting model.

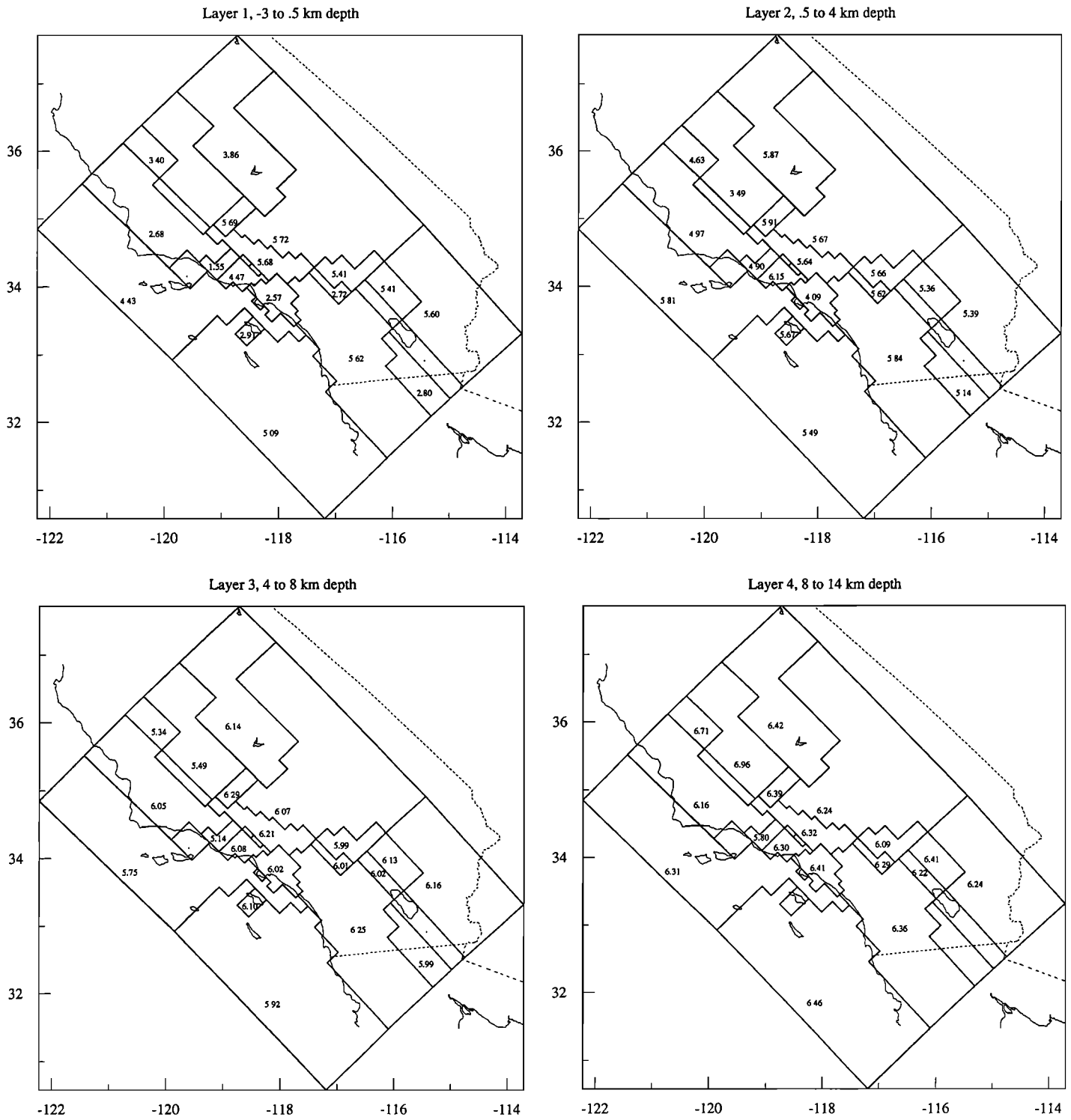

Fig. 10. Results of the inversion (run with station corrections). Each panel represents a different layer and shows P wave velocities in kilometers per second in the appropriate superblock. Blocks with no velocity shown were not inverted. See Figure 1*a* and Table 1 for region names and Table 6 for resolutions.

Most blocks are well resolved. Some, mostly in the top layer and bottom two layers, are not well resolved, due to poor ray coverage. The top layer contains few sources and is sampled mostly by upgoing rays, unlike the other layers, which are also sampled by rays refracting along the layer interfaces. Blocks in the bottom layers contain few sources, and are sampled only by P_n. The P_n coverage may be biased, for example, in a block that is long and narrow in map view, so the P_n arrivals cross only the short dimension of the block; that is, the rays sampling that block are traveling in the same direction. Thus a block may have an adequate hit count but still be poorly sampled. It is also useful to monitor the off-diagonal elements of the resolution matrix. A large off-diagonal element indicates that a block velocity is not isolated from that of another block. This sometimes happened between blocks in the bottom or top two layers of a region, for example in the Coast Ranges west of the San Andreas region.

Another measure of reliability of the results comes from

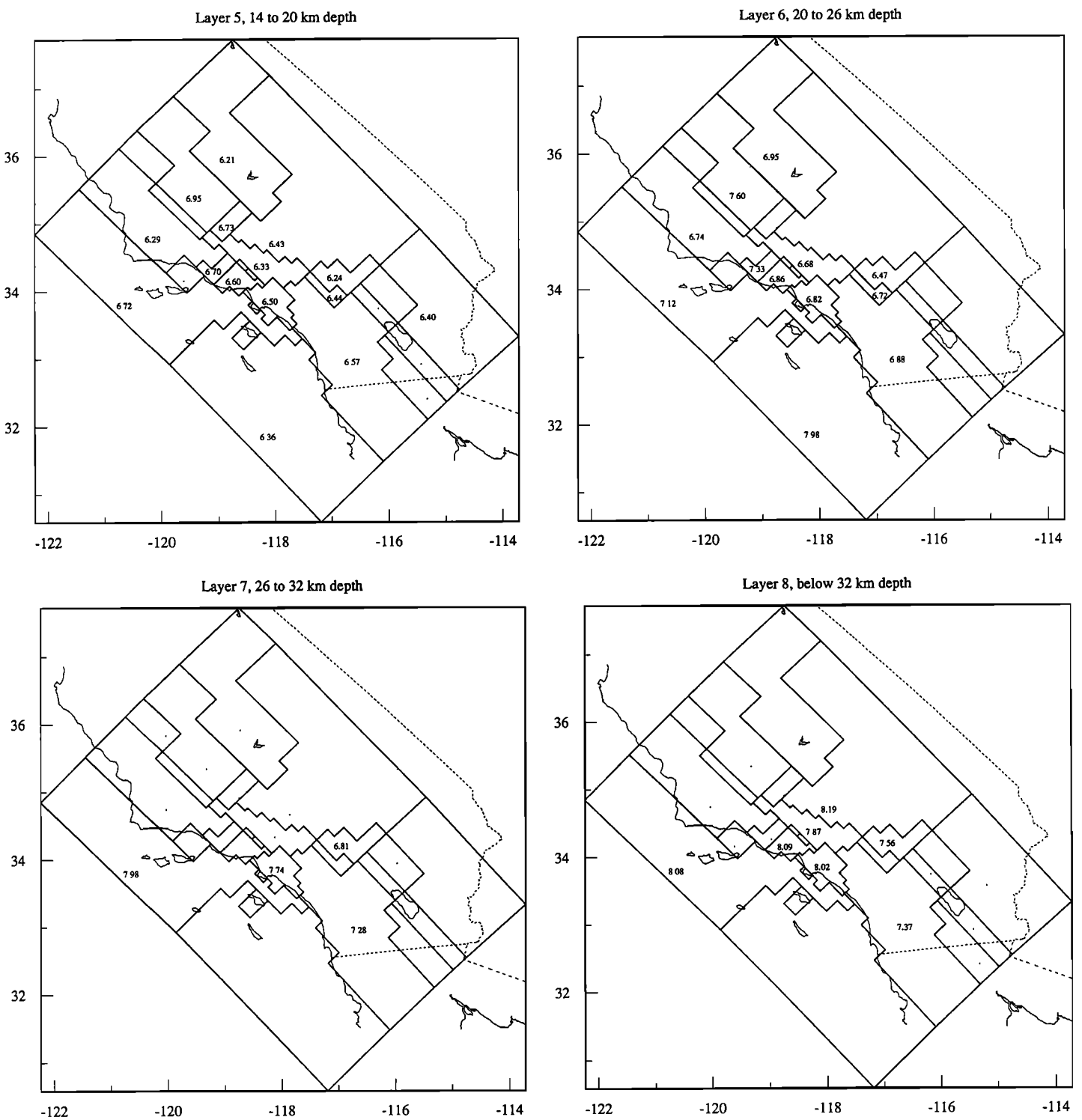

Fig. 10. (continued)

examining the behavior of each block velocity during the inversion process. Velocities of well-behaved blocks were determined during the first two iterations and changed little after that. The results may be considered more robust if the same velocity is determined for a block in each of the two inversion runs (with and without station corrections); for example, most well-resolved blocks in layers representing the middle crust had very similar results from the two runs (Table 5). Most blocks with a resolution greater than about 0.80 had small off-diagonal elements, converged rapidly, and had similar results from the two runs.

To estimate how accurately the velocity of a well-resolved block is determined by the inversion, the following test was made. A well-resolved (resolution=0.99) block representing the Los Angeles basin region at depths of 8 to 14 km was chosen. Both inversion runs agreed on the block's velocity (6.41 and 6.43 km/s). New velocity models were made by changing that block's velocity by ±1%, 5%, and 10%. All the earthquakes were relocated in the new velocity models, and the variance of the travel time residuals in each new model was calculated (Figure 11). About 13% of the rays hit that block. The velocity changes cause large variance increases (comparable to the

variance differences between the inversion iterations shown in Figure 7) and the variance for the actual final velocity is in a well-defined minimum (Figure 11). The width of the minimum suggests that the velocities of the well-resolved blocks are determined to within a few percent.

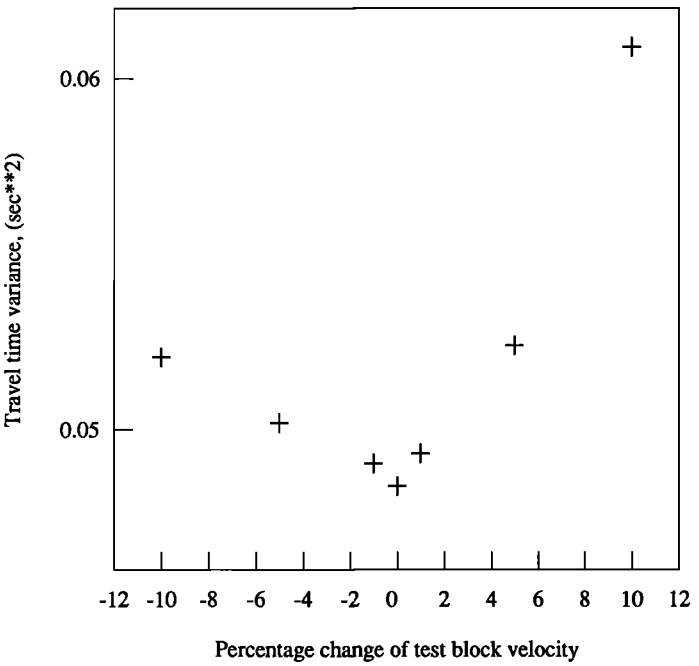

Fig. 11. Variance of all the travel time residuals calculated for velocity models in which the velocity in one block under the Los Angeles basin was perturbed by the amount shown (±1, 5, 10%). See text for discussion.

Another way to judge the inversion results is to see how well the final velocity model fits the explosion travel times. Of course, the explosion travel times were used in the inversion but constituted only a ≈1% of the data used. The Catalina, Whittier Narrows, and Corona explosion travel time residual variances are 6%, 20%, and 31%, respectively, lower in the final model than the starting model (Table 3). The forward three-dimensional model has a lower variance than the inversion result for the Whittier Narrows blast (Table 3) because the forward model allowed the sediment thickness and depth to basement to vary within the Los Angeles basin region. Most of the differences between the forward model and the inverse starting model variances for the Catalina and Corona blasts are due to the distance cutoff used in calculating the variances in the inverse model but not in the forward model.

Discussion

The inversion was successful in determining a crustal *P* wave velocity model that better fit the earthquake travel times. By the measures of the resolution, agreement between the two inversion runs with and without station corrections, and the rapid convergence of the block velocities during the inversion, the blocks representing most of the upper and middle crust were well constrained. In some regions, good control of the lower crustal and Moho velocities was possible.

The variance of the residuals of the *P* wave travel times was reduced by 47% with respect to the starting model during the inversion (Figure 7). Before the inversion, the station corrections lower the variance by accounting for near-station variations in velocity over wavelengths much smaller than the superblock sizes. The variance reduction during the inversion is due to the model's success in improving on the gross regional geologic (and hence velocity) variations initially incorporated into the starting model. Significant variance remains; some must be due to noise in the data, but the rest cannot be reduced by the inversion due to the parameterization of the model. Large blocks are used, but in some areas the geology must vary over scales between that of the superblocks and the station corrections.

It is interesting to make some geologic interpretations of the velocity results (see Figure 1*a* and Table 1 for place names). In the blocks representing the Los Angeles basin region the inversion had good data coverage and resolution, except for the poor resolution of the top block. However, the velocity of that block was well constrained by the Whittier explosion travel time data during the forward modeling. The top layer (from 3 km above sea level to 0.5 km depth), has a *P* wave velocity of 2.6 km/s, typical of unindurated sediments [*Dobrin*, 1976], in agreement with the known surface geology. From 0.5 to 4 km depth the velocity is 4.1 km/s, representing indurated sediments filling the basin. The third layer, from 4 to 8 km depth, has a velocity of 6.0 km/s. Recall that the basin was modeled as having a flat bottom 4 km deep, but it actually varies from 0 to about 10 km depth [*Yerkes et al.*, 1965]. The velocity for this layer can be expected to be an average of the velocities of deeply buried sediments and the basement rocks on which the sediments lie. The crustal velocity structure between 8 and 26 km under the Los Angeles basin is very similar to that under the Peninsular Ranges (Table 5 and Figure 10). This strongly suggests that the basin is underlain by plutonic rocks of the Peninsular Ranges batholith. The three-dimensional model does not attempt to split the Los Angeles basin along the Newport-Inglewood fault, which may separate different basement rock types [*Yerkes et al.*, 1965]. Most of the rays sample the basin basement east of the fault so the inferred granitic basement may lie only to the east of the fault. A granitic basement between 8 and 26 km depth under the Santa Monica Mountains is also suggested by velocities comparable to those under the Los Angeles basin and Peninsular Ranges. The Los Angeles basin layer from 26 to 32 km depth has a velocity of 7.7 km/s, nearly a typical Moho velocity. One possibility is that the Moho is between 26 and 32 km depth and the 7.7 km/s velocity represents an average of the lower crustal and Moho velocities. This is a shallower Moho than determined by *McCulloh* [1960], who used gravity data to model a gently east dipping Moho 32 km deep under the central Los Angeles basin. The velocity of the lowest layer, deeper than 32 km, is 8.0 km/s representing the uppermost mantle.

In contrast with the Los Angeles basin, the Ventura basin region lacks velocities indicative of granitic rocks. From 4 to 14 km depth, velocities are lower, and from 14 to 26 km depth, velocities are higher, in the Ventura basin than velocities at corresponding depths under the Los Angeles basin (Table 5 and Figure 10). Although velocities are not determined below 26 km, the results indicate a more mafic, possibly oceanic crust below the Ventura basin, similar to that underlying the Great Valley [e.g., *Crouch*, 1981]. The velocity contrast between layers 5 and 6 of the Ventura basin and the Great Valley is the same, 0.6 km/s, suggesting the same lithologic contrast in both regions. This contrast is not seen in any other region. The absolute velocities of those layers differ in the two regions due,

we think, to the same lithologies being deeper in the Ventura basin than in the Great Valley, so that the velocities averaged within the fixed block interfaces differ.

The velocity results for the Peninsular Ranges are robust but are curious for the lowest layers, representing depths from 26 to below 32 km (Table 5 and Figure 10). The velocity at that depth range, about 7.3 km/s, is not typical of crustal or upper mantle rocks but probably represents an average of the two. The large depth range over which the velocity averaging occurs implies either a very irregular bottom of the crust, with both upper mantle and lower crustal material present in that depth range, or a dipping Moho. An eastward dip of 3.5° over the ≈100 km width of the Peninsular Ranges could account for the velocity averaging. The velocities determined for the Peninsular Ranges are similar to the velocities found in the few well-resolved blocks representing the Sierra Nevada region.

For the San Gabriel Mountains region the velocities (Table 5, note that layer 7 has poor resolution) and depth to Moho (about 32 km depth, based on the velocity of layer 8) found here differ little from those of *Hadley and Kanamori* [1977], from whom the starting model was taken. At every depth, the San Bernardino Mountains region has slightly lower velocities than the San Gabriel Mountains and has a thicker zone of velocities in the low 6 km/s range, also in general agreement with *Hadley and Kanamori* [1977]. The lower velocity of layer 8 under the San Bernardino Mountains may signify either lower upper mantle velocities or a deeper, or dipping, Moho.

The continental borderland provinces have sparse seismograph coverage, but the blocks representing the north continental borderland were well resolved. The crust above 20 km depth has velocities typical of many of the onshore regions (Table 5 and Figure 10). The velocities below 26 km depth are upper mantle velocities, with the Moho between 20 and 26 km depth, as indicated by an intermediate velocity. Thus this region can be described as thinned continental crust. The Moho depth and crustal velocities found here agree well with the results of *Keller and Prothero* [1987].

The results from this study agree generally with the tomographic inversion of *Hearn and Clayton* [1986*a*,*b*] using similar data. Their largest late P_g arrivals occur in the Los Angeles and Ventura basins, which have the slowest shallow velocities found in this study. Both studies have, at 10 km depth (Table 5 and Figure 10, layer 4), the San Bernardino Mountains slower than the San Gabriel Mountains and a relatively slow Mojave, and each study finds that the Peninsular Ranges, Los Angeles basin, and San Gabriel Mountains have similar velocities at that depth. Both studies find P_n velocities that are relatively high (>7.8 km/s) under the Los Angeles basin and Mojave, relatively low (<7.8 km/s) under the Peninsular Ranges and San Bernardino Mountains, and near 7.8 km/s under the San Gabriel Mountains. The Tehachapi, San Gabriel, and San Bernardino mountains appear to have distinct identities at 10 km depth in the current study where *Hearn and Clayton* [1986*a*] interpret these mountains as being rootless. This difference may be due to the different model parameterizations.

Earthquake relocations in the inverse model

To demonstrate the utility of the inverse three-dimensional model, we relocate 98 $M_L \geq 4$ earthquakes in the three-dimensional model and compare the relocations to the catalog locations. A few of the relocated earthquakes have been subject to special studies including relocations in local velocity models. The relocations here are not meant as the final word on the earthquake locations but only to demonstrate the usefulness of the inverse three-dimensional model for routine earthquake location.

The earthquakes were recorded on the USGS-Caltech seismic network in southern California. Arrival times and catalog hypocenters come from the routine processing [*Given et al.*, 1986] of the recorded events. The $M_L \geq 4$ earthquakes were arbitrarily selected from the Caltech catalog; each event was between 1978 and 1988 and has 10 or more P and S wave phase picks and good azimuthal coverage by the network. Earthquakes that had been used in the inversion to generate the model were discarded. The magnitude cutoff was chosen only to limit the number of events to be relocated.

The earthquakes are relocated in the inverse three-dimensional velocity model (found with station delays) with a cutoff for distance downweighting of 100 km. This cutoff eliminates rays that traveled through the blocks representing the lower portions of the model that were not well constrained. Arrivals with large residuals are also downweighted, with the residual cutoff set from 3 to 1 s for the first to last iteration of the location program. S wave arrivals are given one-half the weight of P wave arrivals, and a V_p/V_s ratio of 1.73 is assumed, but only 1.6% of the arrivals used were S waves.

The earthquakes relocated in the three-dimensional model have a P wave residual variance 44% lower than the catalog locations in the standard one-dimensional model (Table 3). Earthquake epicenters usually change little during relocation, typically less than 2 km. Depths typically change by several kilometers. In regions topped by seismically slow sediments (the Los Angeles basin, Great Valley, Imperial Valley, Coachella Valley, Borrego Valley, and Santa Barbara Channel), containing 43 of the 98 events, the earthquake depths increased by an average of 2.4 km (Figure 12). The events outside these regions had depths decrease by an average of 2.0 km. The relocations of the 1987 M_L 5.9 Whittier Narrows earthquake and its M_L 5.3 largest aftershock are very near (<1 km in latitude and longitude and <2 km in depth) to the carefully determined locations of those events found by *Hauksson and Jones* [1989] using a hybrid one-dimensional velocity model and station corrections.

CONCLUSIONS

The use of a three-dimensional P wave velocity model of the southern California crust significantly reduces the variance of travel time residuals for local earthquakes and allows the identification of rock types within the crust.

We constructed a three-dimensional model composited from one-dimensional structures available for geologic provinces within southern California and calibrated the model with explosion travel times. The model reduces the variance of P wave travel time residuals of Los Angeles basin earthquakes by half from the standard one-dimensional structure. The new earthquake locations cluster more tightly and contain fewer artifacts than the catalog locations.

An eight-layer model encompassing all of southern California was determined from the first arrivals of ≈1000 well-located earthquakes. This model yields similar improvements in earthquake location, reducing the P wave travel time variance of 98 larger ($M_L \geq 4$) earthquakes by about half from that of the standard one-dimensional model. The P wave velocity results are useful in determining rock types within the crust; for

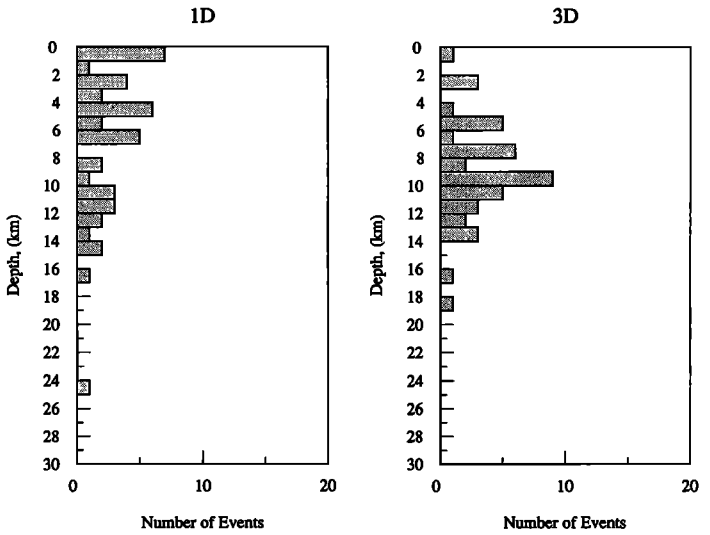

Fig. 12. Depth distributions of some earthquakes from the catalog (left) and after relocation (right) in the final inverse three-dimensional velocity model. The depths are of earthquakes in the Los Angeles basin, Coachella Valley, Borrego Valley, Great Valley, Imperial Valley, and Santa Barbara Channel provinces, selected from the 98 relocated $M_L \geq 4$ earthquakes because they occurred in areas of large velocity contrasts. 60% of the catalog depths are above 7 km and 74% of the three-dimensional relocations are below 7 km.

example, we found that beneath the Los Angeles basin most of the basement rocks have velocities similar to the granitic rocks of the Peninsular Ranges and that the Moho is shallower than 32 km. In contrast, the velocities found under the Ventura basin indicate granitic rocks are absent there. Other interpretations of the *P* wave velocities may help constrain models of the crustal evolution of southern California.

These results underscore the limitations of a one-dimensional velocity model when examining earthquakes over an area of such diverse geology as southern California. Substantial changes in hypocenter locations, especially in depth, can result from shifting from a one- to a three-dimensional structure; these changes often exceed the standard errors computed in a one-dimensional structure. Use of these three-dimensional models should improve earthquake locations, and hence our understanding of seismogenic structures, throughout southern California.

Acknowledgments. We thank Steve Roecker for the use of his codes and Rob Clayton for the use of his earthquake data base and sorting routines. Egill Hauksson provided additional Whittier Narrows blast arrival times. Marianne Walck and an anonymous reviewer provided helpful reviews. This work was supported by the U.S. Geological Survey under contract 14-08-0001-G1774. Contribution 5013, Division of Geological and Planetary Sciences, California Institute of Technology.

REFERENCES

Abers, G. A., and S. W. Roecker, Deep structure of an arc-continent collision: Earthquake relocation and inversion for upper mantle *P* and *S* wave velocities beneath Papua New Guinea, *J. Geophys. Res., 96*, 6379-6401, 1991.

Colburn, R. H., and W. D. Mooney, Two-dimensional velocity structure along the synclinal axis of the Great Valley, California, *Bull. Seismol. Soc. Am., 76*, 1305-1322, 1986.

Corbett, E. J., Seismicity and crustal structure studies of southern California: Tectonic implications from improved earthquake locations, Ph.D. thesis, 231 pp., Calif. Inst. of Technol., Pasadena, 1984.

Corbett, E. J., and C. E. Johnson, The Santa Barbara, California, earthquake of 13 August 1978, *Bull. Seismol. Soc. Am., 72*, 2201-2226, 1982.

Crandell, G. J., B. P. Luyendyk, M. S. Reichle, and W. A. Prothero, A marine seismic refraction study of the Santa Barbara channel, California, *Mar. Geophys. Res., 6*, 15-37, 1983.

Crouch, J. K., Northwest margin of California continental borderland--Marine geology and tectonic evolution, *AAPG Bull., 65*, 191-218, 1981.

Davis, T. L., J. Namson, and R. F. Yerkes, A cross section of the Los Angeles area: Seismically active fold and thrust belt, the 1987 Whittier Narrows earthquake, and earthquake hazard, *J. Geophys. Res., 94*, 9644-9664, 1989.

Dobrin, M. B., *Introduction to Geophysical Prospecting*, McGraw-Hill, New York, 1976.

Eaton, J. P., M. E. O'Neill, and J. N. Murdock, Aftershocks of the 1966 Parkfield-Cholame, California, earthquake: A detailed study, *Bull. Seismol. Soc. Am., 60*, 1151-1197, 1970.

Eberhart-Phillips, E., Active faulting and deformation of the Coalinga anticline as interpreted from three-dimensional velocity structure and seismicity, *J. Geophys. Res., 94*, 15,565-15,586, 1989.

Eberhart-Phillips, E., A. J. Michael, G. Fuis, and R. Luzitano, Three-dimensional crustal velocity structure in the region of the Loma Prieta, California, earthquake sequence from inversion of local earthquake and shot arrival times (abstract), *Seismol. Res. Lett., 61*, 48, 1990.

Fuis, G. S., W. D. Mooney, J. H. Healey, G. A. McMechan, and W. J. Lutter, Crustal structure of the Imperial Valley region, in The Imperial Valley, California, Earthquake of October 15, 1979, *U.S. Geol. Surv. Prof. Pap. 1254*, 25-50, 1982.

Given, D. D., and C. L. Koesterer, Station arrival data for a quarry blast on Santa Catalina Island, California, *U.S. Geol. Surv. Open File Rep., 83-462*, 12 pp., 1983.

Given, D. D., R. Norris, L. M. Jones, L. K. Hutton, C. E. Johnson, and S. Hartzell, The southern California network bulletin January through June, 1986, *U.S. Geol. Surv. Open File Rep., 86-598*, 28 pp., 1986.

Given, D. D., L. Wald, L. M. Jones, and L. K. Hutton, The southern California network bulletin July through December, 1987, *U.S. Geol. Surv. Open File Rep., 89-323*, 34 pp., 1989.

Hadley, D. M., Geophysical investigations of the structure and tectonics of southern California, Ph.D. thesis, 167 pp., Calif. Inst. of Technol., Pasadena, 1978.

Hadley, D., and J. Combs, Microearthquake distribution and mechanisms of faulting in the Fontana-San Bernardino area of southern California, *Bull. Seismol. Soc. Am., 64*, 1477-1499, 1974.

Hadley, D., and H. Kanamori, Seismic structure of the Transverse Ranges, California, *Geol. Soc. Am. Bull., 88*, 1469-1478, 1977.

Hamilton, R. M., Time term analysis of explosion data from the vicinity of the Borrego Mountain, California, earthquake of 9 April 1968, *Bull. Seismol. Soc. Am., 60*, 367-381, 1970.

Hauksson, E., Seismotectonics of the Newport-Inglewood fault zone in the Los Angeles basin, southern California, *Bull. Seismol. Soc. Am., 77*, 539-561, 1987.

Hauksson, E., and L. M. Jones, The 1987 Whittier Narrows earthquake sequence in Los Angeles, southern California: Seismological and tectonic analysis, *J. Geophys. Res.*, *94*, 9569-9590, 1989.

Healy, J. H., Crustal structure along the coast of California from seismic refraction measurements, *J. Geophys. Res.*, *68*, 5777-5787, 1963.

Hearn, T. M., and R. W. Clayton, Lateral velocity variations in southern California. I. Results for the upper crust from P_g waves, *Bull. Seismol. Soc. Am.*, *76*, 495-510, 1986*a*.

Hearn, T. M., and R. W. Clayton, Lateral velocity variations in southern California. II. Results for the lower crust from P_n waves, *Bull. Seismol. Soc. Am.*, *76*, 511-520, 1986*b*.

Johnson, C. E., CEDAR--An approach to the computer automation of short-period local seismic networks, Ph.D. thesis, 332 pp., Calif. Inst. of Technol., Pasadena, 1979.

Jones, L. M., and R. S. Dollar, Evidence of basin-and-range extensional tectonics in the Sierra Nevada: The Durrwood Meadows swarm, Tulare County, California (1983-1984), *Bull. Seismol. Soc. Am.*, *76*, 439-461, 1986.

Kanamori, H., and D. Hadley, Crustal structure and temporal velocity change in southern California, *Pure Appl. Geophys.*, *113*, 257-280, 1975.

Keller, B., and W. Prothero, Western Transverse Ranges crustal structure, *J. Geophys. Res.*, *92*, 7890-7906, 1987.

Lees, J. M., Comparison of high resolution tomographic *P* wave inversions at Parkfield and Loma Prieta, California (abstract), *Seismol. Res. Lett.*, *61*, 49, 1990.

Lees, J. M., and C. Nicholson, High resolution travel-time tomography in the northern Coachella Valley from inversion of aftershock arrival times of the 1986 M_L 5.9 North Palm Springs earthquake (abstract), *Seismol. Res. Lett.*, *61*, 48, 1990.

Magistrale, H., L. Jones, and H. Kanamori, The Superstition Hills, California, Earthquakes of 24 November 1987, *Bull. Seismol. Soc. Am.*, *79*, 239-251, 1989.

McCulloh, T. H., Gravity variations and the geology of the Los Angeles basin of California, *U.S. Geol. Surv. Prof. Pap.*, *400-B*, 320-325, 1960.

Michelini, A., W. Foxall, and T. McEvilly, The Parkfield monitoring program: Joint hypocentral and velocity inversion for three-dimensional structure (abstract), *Seismol. Res. Lett.*, *60*, 31, 1989.

Michelini, A., W. Foxall, and T. McEvilly, Loma Prieta sequence: Joint inversion for 3-D velocity structure and faulting geometry (abstract), *Seismol. Res. Lett.*, *61*, 48, 1990.

Perkins, G., Data report for the 1987 seismic calibration/refraction survey, Whittier, California, 29 pp., U.S. Geol. Surv., Menlo Park, Calif., 1988.

Robertson, M., and E. Hauksson, Three-dimensional fine velocity structure of the Los Angeles basin (abstract), *Eos Trans. AGU*, *70*, 1192, 1989.

Roecker, S. W., Seismicity and tectonics of the Pamir-Hindu Kush region of central Asia, Ph.D. thesis, 298 pp., Mass. Inst. of Technol., Cambridge, 1981.

Roecker, S. W., Velocity structure of the Pamir-Hindu Kush region: Possible evidence of a subducted crust, *J. Geophys. Res.*, *87*, 945-959, 1982.

Roecker, S. W., Y. H. Yeh, and Y. B. Tsai, Three-dimensional *P* and *S* wave velocity structures beneath Taiwan: Deep structure beneath an arc-continent collision, *J. Geophys. Res.*, *92*, 10,547-10,570, 1987.

Shedlock, K. M., Structure and tectonics of north China, Ph.D. thesis, 194 pp., Mass. Inst. of Technol., Cambridge, 1986.

Shedlock, K. M., and S. W. Roecker, Elastic wave velocity structure of the crust and upper mantle beneath the North China basin, *J. Geophys. Res.*, *92*, 9327-9350, 1987.

Stierman, D. J., and W. L. Ellsworth, Aftershocks of the February 21, 1973 Point Mugu, California earthquake, *Bull. Seismol. Soc. Am.*, *66*, 1931-1952, 1976.

Thurber, C. H., Earthquake locations and three-dimensional crustal structure in the Coyote Lake area, central California, *J. Geophys. Res.*, *88*, 8226-8236, 1983.

Thurber, C., and W. L. Ellsworth, Rapid solution of ray tracing problems in heterogeneous media, *Bull. Seismol. Soc. Am.*, *70*, 1137-1148, 1980.

Walck, M. C., and R. W. Clayton, *P* wave velocity variations in the Coso region, California, derived from local earthquake travel times, *J. Geophys. Res.*, *92*, 393-405, 1987.

Walter, A. W., and W. D. Mooney, Crustal structure of the Diablo and Gabilan ranges, central California: A reinterpretation of existing data, *Bull. Seism. Soc. Am.*, *72*, 1567-1590, 1982.

Yerkes, R. F., T. H. McCulloh, J. E. Schoellhamer, and J. G. Vedder, Geology of the Los Angeles basin, California--An introduction, *U.S. Geol. Surv. Prof. Pap.*, *420-A*, 1-57, 1965.

C. Jones, Mackay School of Mines, University of Nevada, Reno, NV 89557.

H. Kanamori, Seismological Laboratory, Division of Geological and Planetary Sciences, California Institute of Technology, Pasadena, CA 91125.

H. Magistrale, Department of Geological Sciences, San Diego State University, San Diego, CA 92182.

(Received September 4, 1991;
revised February 13, 1992;
accepted February 19, 1992.)